

# **Contents**

Pot in Pot Refrigerator ( 4-6)
Spaghetti Accelerator(7-10)
The Effect of Different Salts on(11-14)
Investigation of Lato Lato Oscillation(15-18)
Strange Motion(19-20)
Magnetic Assist(21-26)
Construction of a Four - Gel Vertical (27- 28)
Investigation of a Fluid in a High Voltage(29- 32)
Rotating Ring( 33-37)
Watercourse Blockage Detection System(38-40)
Continue I bustonesis

# **Editor in Chief**

Dr. Dina Izadi
Physics Education, National Polytechnic Institute
IPN, Mexico
Researcher & President, AYIMI & ADIB
info@ayimi.org
dinaocean@gmail.com

# **Associated Editors**

Professor Masoud Torabi Azad Physical Oceanography, Azad University & Board Member, AYIMI torabi us@yahoo.com

Nona Izadipanah
Geophysicist, Scientific Committee &
Board Member, AYIMI
daisyip67@gmail.com

Professor Cesar Eduardo Mora Ley Physics Education, National Polytechnic Institute, IPN, and CICATA Principal, Mexico ceml36@gmail.com

Dorna Izadipanah
Microbiologist, Medical Diagnosis Laboratory
Scientific Committee &
Board Member, AYIMI
dorna\_izadipanah@yahoo.com

Dr. Carmen del Pilar Suarez Rodriguez Faculty Member, Physics Education, UASLP, Universidad Autónoma de San Luis Potosí, Mexico pilar.suarez@uaslp.mx

# Young Scientist Research

Title proper: Young Scientist Research

**Subject**: NATURAL SCIENCES, ART, ENGINEERING AND TECHNOLOGY

Corporate contributor: Ariaian Young

Innovative Minds Institute

Publisher: Tehran: Ariaian Young

**Innovative Minds Institute** 

**Dates of publication:** 2017- Present

Frequency: Annual

Type of resource: Periodical

Language: English

Country: Iran

Medium: Online

**Indexed by:** ROAD (The Directory of Open Access Resources)

ISSN- 2588-5111 ISSN International Centre 45 rue de Turbigo 75003 Paris France

# Address:

Unit 14, No.32, Malek Ave., Shariati St.

Post Code: 1565843537

Tel:+9821-77507013, 77522395

Copyright © Ariaian Young Innovative Minds Institute, AYIMI http://journal.ayimi.org

# WELCOME TO THE INTERNATIONAL JOURNAL of YOUNG SCIENTIST RESEARCH

Young Scientist Research is a research journal based on scientific projects and we are pleased to present our students' work in scientific activities. This open-access journal includes young students' research in any field of science which publishes full-length and abstract research on any aspects of applied sciences in relation to work presented in both national and international conferences, competitions and tournaments of all types.

Programs that have educational opportunities for high school students to present their distinguished projects from regional, national and international events such as International Conference of Young Scientists (ICYS), International / Persian Young Physicists' Tournament (IYPT/ PYPT), International / Iran Physics' Tournament (IPT/ IRPT), International / Persian Young Naturalists' Tournament (IYNT/ PYNT) and International ISAC Olympiad.

New manuscripts sent to the Journal will be handled by the Editorial Office who checks compliance with the guidelines to authors. Then a rapid screening process at which stage a decision to reject or to go to full review is made.

By submission of a manuscript to the Journal, all authors warrant that they have the authority to publish the material and that the paper, or one substantially the same, has neither been published previously, nor is being considered for publication elsewhere.

This journal belongs to Ariaian Young Innovative Minds Institute, AYIMI, and one to two issues are published in a year. All details are on the YOUNG SCIENTIST RESEARCH Journal website (http://journal.ayimi.org).

Editor in Chief
Dr. Dina Izadi
Researcher & President of
Ariaian Young Innovative Minds Institute, AYIMI
ADIB, Cultural and Artistic Institute
<a href="http://www.ayimi.org">http://www.ayimi.org</a>
<a href="http://journal.ayimi.org">http://journal.ayimi.org</a>
Email: <a href="mailto:info@ayimi.org">info@ayimi.org</a>
Unit 14, No. 32, Malek Ave., Shariati St.,

Post Code: 1565843537, Tehran/ Iran

Young Scientist Research Journal, ISSN: 2588-5111



CURRENT ISSUE Vol 9 NO2 August 2025

COPYRIGHT © INTERNATIONAL JOURNAL OF YOUNG SCIENTIST RESEARCH (http://journal.ayimi.org)

# **POT IN POT REFRIGERATOR**

Natalia Ruzickova, Michal Hledík Boris Vavrík, Slovakia

#### ABSTRACT

#### ARTICLE INFO

Slovakia Team Membes in IYPT 2014, UK

Accepted by Ariaian Young Innovative

Minds Institute, AYIMI

http://www.ayimi.org,info@ayimi.org

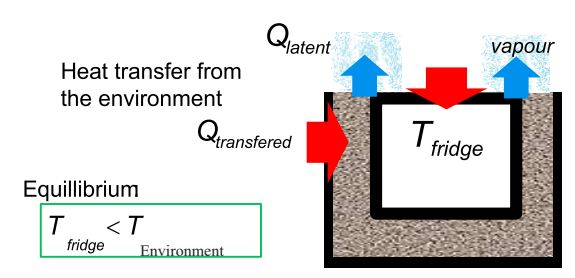
he Pot in Pot refrigerator is a device to keep foods cool using the principle of evaporative cooling. It consists of a pot placed inside a bigger pot with the space between them filled with a wet porous material, e.g. sand. How might one achieve the best cooling effect? Low temperature or fast cooling? Here the effective parameters are studied.

Key Words: Pot in Pot, Cooling, Porous Material

# 1. Introduction

The mechanism of the pot in pot refrigerator and wet porous materials are:

· Evaporation, latent heat and cooling



A granular material which is used between two pots is sand. The smaller pot which is inside the bigger one keeps the temperature low enough for cooling system.

Big granules:

- · Better airflow
- Water drains down

Small granules:

- Can soak with water
- Little space for airflow

Comparing with other kind of porous material such as cloth which gets soaked with water and can be exposed to air flow on sufficient area (Fig. 1):

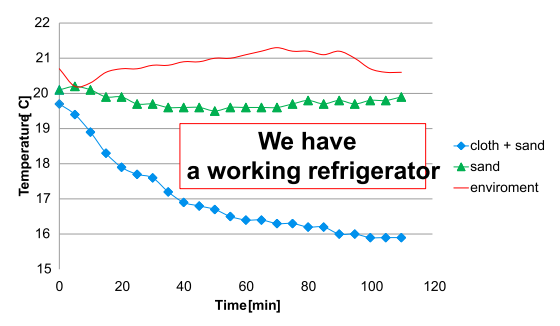


Fig. 1: The difference between cloth and sand

How might one achieve the best cooling effect? Low temperature or fast cooling?

By Simple model of the cooling, Experimentally

verification and optimization we are going to estimate the best possible cooling.

# 2. Model of the Cooling

• Evaporation rate:

dm = ASvdt

A: related to volatility of the liquid (in air)

• Heat transferred from the surroundings:

 $dQ = BSv\Delta Tdt$ 

B: related to thermal conductivity, capacity of air

S Surface area

v Air flow speed

 $\Delta T$  Temperature difference

#### 2.1. Calorimetry:

 $ASv\lambda dt - BSv\Delta Tdt = -CdT$ 

$$T = T_{air} - \frac{A\lambda}{B} \left( 1 - e^{-\frac{BSv_r}{C}t} \right)$$

Final temperature drop:  $\Delta T = \frac{A\lambda}{R}$ 

Speed of cooling:  $\frac{BSV}{}$ 

С

 $\lambda$  = latent heat

C = thermal capacity of fridge

# 3. Experiment Verification

# 3.1. High vs. Low Outer Pot

Terminal temperature depends on materials only:

$$\Delta T = \frac{A\lambda}{B}$$

Cooling rate:

$$\frac{BSV}{C} \qquad \text{more water} \rightarrow \text{bigger} C \rightarrow \text{slower cooling}$$

By comparing high versus low pot both models show the same terminal temperature.

The rate of cooling shows:

Low outer pot: Less water, then smaller thermal capacity, and faster cooling

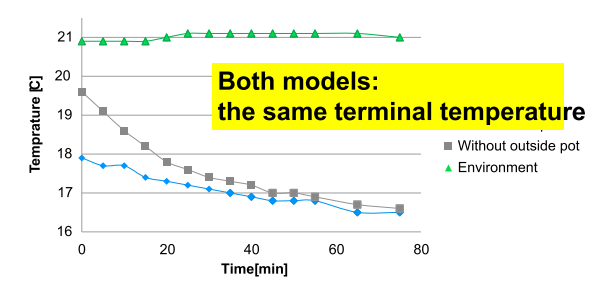


Fig. 2: High vs. low pot: final temperature

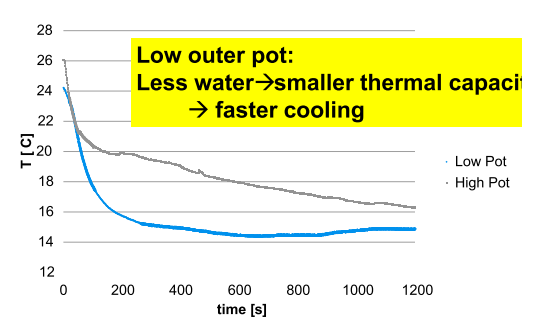


Fig. 3: Comparing rate of cooling, High vs. low pot

# 3.2. Size and Shape of the Fridge

Terminal temperature:

$$\Delta T = \frac{A\lambda}{B}$$

BSv

С

Speed of cooling which is independent of size/shape:

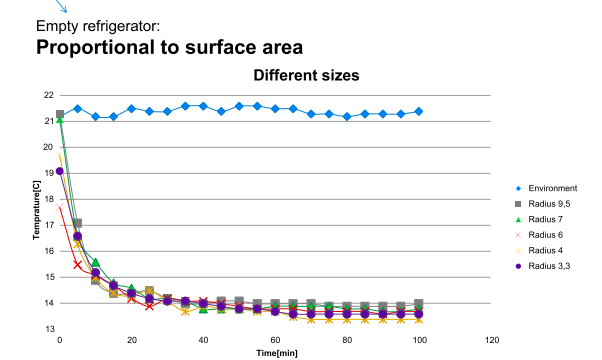


Fig. 4: Effect of different sizes

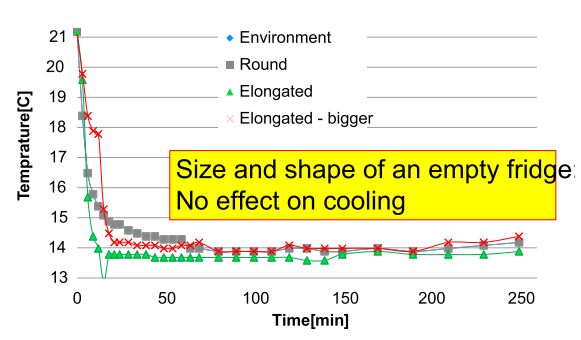


Fig. 5: Effect of different shapes

#### 3.3. What's Inside?

According to the terminal temperature, it is independent from content but speed of cooling shows in high capacity it cools slower.

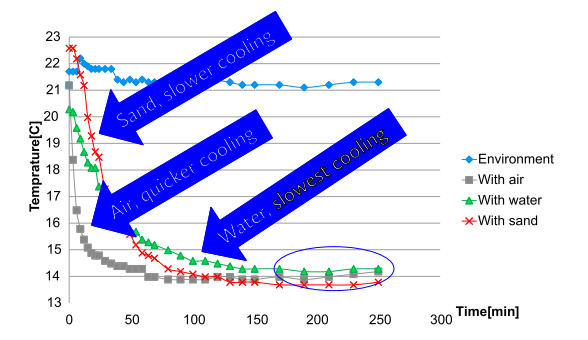


Fig. 6: Changing heat capacity of the fridge

Bigger capacity makes slower cooling but no effect on final temperature.

#### 3.4. Different Liquids

Terminal temperature grows with volatility and latent

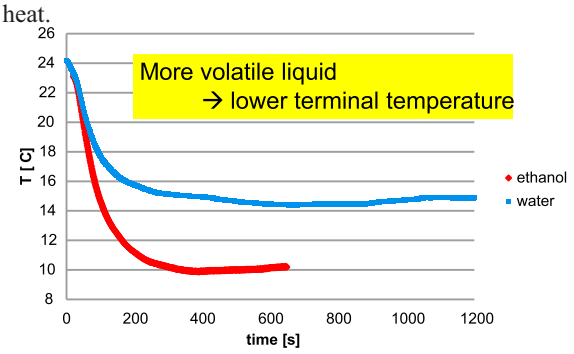
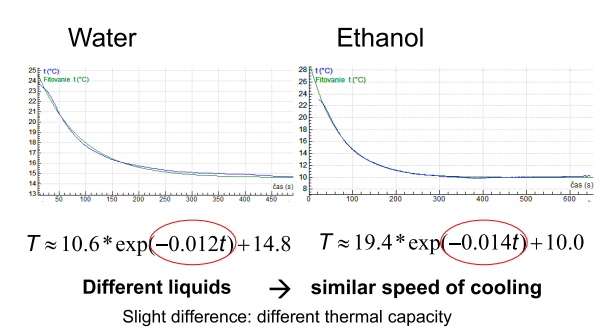
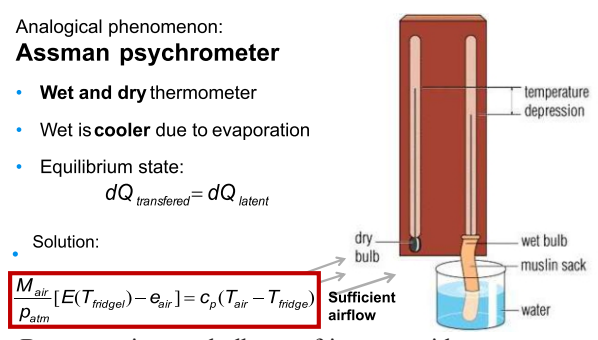


Fig. 7: Water VS. Ethanol



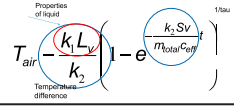
# 4. What is the Best Possible Effect?

Minimal temperature estimation:



By comparing wet bulb vs. refrigerator with temperature vs. time diagram we can get close to the theoretical minimum.

Speed of Cooling:



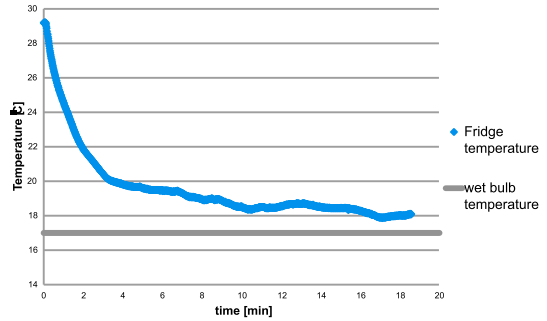


Fig. 8: Wet bulb vs. refrigerator

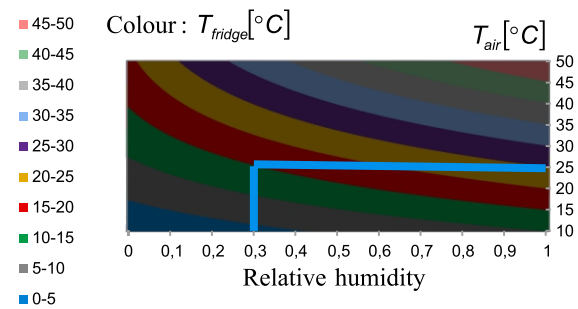
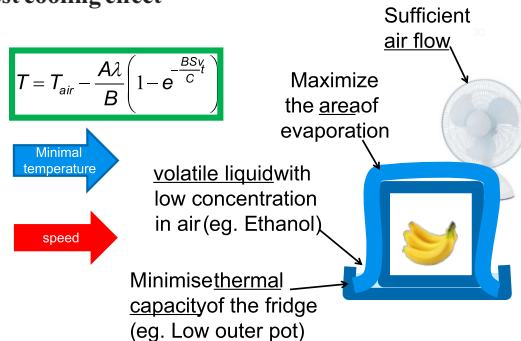


Fig. 9: Minimal achievable temperature

# Best cooling effect



# Assman psychrometer: Theory

Equillibrium of heat flow:

$$dQ_{transfered} = dQ_{latent}$$

$$dQ_{transfered} = dm_{air}c_{air}(T_{air} - T_{fridge})$$

$$dQ_{latent} = dm_{water}L_v$$

Air cools to Tfridge; vapor pressure saturates:

$$dQ_{latent} = \frac{nM\lambda}{p} \Big( E \Big( T_{fridge} \Big) - e \Big)$$

$$dQ_{transfered} = nc_p (T_{air} - T_{fridge})$$

$$\frac{M_{air}}{p_{air}}[E(T_{fridgel}) - e_{air}] = c_p(T_{air} - T_{fridge})$$

Surrounding air:

- Transfers heat to the cloth:

$$dQ_{transfered} = dm_{ir}c_{air}(T_{air} - T_{fridge})$$

$$dQ_{tatent} = dm_{water}L_{v}$$

Absorbs water vapor (heat used for evaporation) Equilibrium (terminal temperature):

$$dQ_{transfered} = dQ_{tatent}$$

#### 5. conclusion

- Minimal temperature:
- sufficient air flow, maximize evaporation area
- volatile liquid with low concentration in air (eg. Ethanol)
- Fastest cooling:
- -Fast air flow
- -Minimise thermal capacity of the fridge (eg. Low outer pot)
- Prediction of minimal temperature

$$T = T_{air} - \frac{A\lambda}{B} \left( 1 - e^{\frac{BSV_i}{C}} \right)$$

# **SPAGHETTIACCELERATOR**

Elina Rouhi, Farzanegan 2 high school, elinarouhi 1388@gmail.com

# ARTICLE INFO

a) Iran team member, IYPT 2025, Lund University Sweden Supervisos: Mohammad Mahdi Sharatmadar,

Alireza Noroozshad

Accepted by Ariaian Young Innovative

Minds Institute, AYIMI

http://www.ayimi.org,info@ayimi.org

#### ABSTRACT

hen a piece of spaghetti is pushed into a bent tube, small debris of spaghetti may be ejected from the other end of the tube at a surprisingly high speed. To model and understand the phenomenon, several important parameters are considered: the projectile's length and mass which was dependent, Young's modulus of spaghetti, tube inner & outer diameter, the tube material and the bending angle of the tube. These variables affect energy storage and its releasing during the process. Moving to solving this problem, foundational concepts relevant to this phenomenon are discussed both theocratically and experimentally.

Keywords: Spaghetti, Debris, Ejection, Accelerator

#### 1. Introduction

The mechanical stability of constrained spaghetti has been studied in spaghetti accelerator. The physical process of fragmentation is relevant to several areas of science and technology to find relevant parameters includes: surface energy contributions, nucleation and growth properties of the fracture process, elastic buckling, and stress wave propagation.

The mechanical strength of dry spaghetti is ordinarily used as a standard of quality control because it is closely related to the semolina properties (mainly gluten content) and to the pasta processing, specially to the drying step (which has proved critical to the quality of the final product). In addition, mechanical measurements are simple and can be easily integrated in the production plant, and provide useful information for the design of packing and shipping operations.

To assess the mechanical performance of dry spaghetti, flexural tests and compression tests (where the final collapse is due to fiber buckling) are usually performed. A nominal rupture strength is obtained from the tests by dividing the maximum load recorded by the cross sectional area of the specimen.

Let's now analyze the ejected debris mechanism. Dry spaghetti behaves like a slender brittle beam. We modeled it as an elastic rod constrained by the tube. First of all, when we push the spaghetti in tube, we have force transmission and localized fracture initiation. Which bends the spaghetti and stored potential energy in it. Then fracture occurred and the potential energy converted into kinetic energy of the fragments and then the spaghetti debris ejected at high speed.



- 1 Force Transmission and Localized Fracture Initiation
- **2** Fracture-Induced Impacts and Energy Transfer
- 3 Ballistic Ejection of Debris

Our experimental setup, includes a fixed stand to hold and stabilize the tube during the experiment, spaghetti, a tube, and a linear actuator that we use to maintain a constant input speed of the spaghetti (Fig. 2).





Arduino Nano



Linear Actuator

The state of the s

-

Fig. 2: Experimental setup

Aa linear actuator, Arduino nano, was used for controlled motion & insertion speed.

Fragment velocities was measured using Tracker application. The calibration was done by sticking to the diameter of the tube to manually track the fragments center at each frame (Fig. 3).



Fig. 3: Tracking the fragments

MATLAB is used for numerical calculation and video processing for the exit velocity of the fragments.

Fig. 1: Ejected debris mechanism

# 2. Experiment

#### 3. Qualitative Analysis

Our preliminary hypothesis is that the spaghetti undergoes elastic deformation inside the curved tube. When it is unable to bend any further, it fractures. This sudden release of stored elastic energy causes debris to be ejected with high speed (Fig. 4).

So, our central idea is: Elastic deformation stores energy.

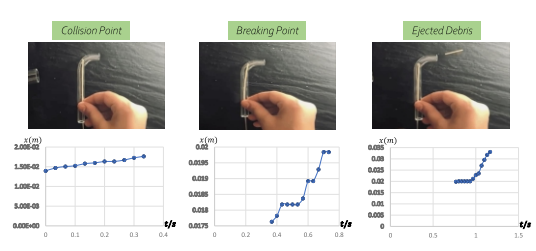


Fig. 4: Condition of Breaks

Also we analyzed the length of the fragments while changing the bending angle. As you can observe, when the bending angle of the tube increases the fragments are smaller and the length of debris decreases (Fig. 5).

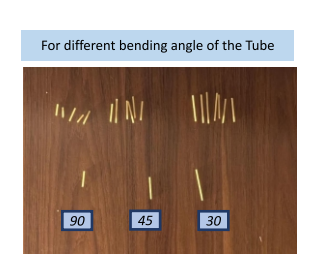




Fig. 5: Fragments length

Let's now analyze the spaghetti breaking mechanism.

- 1 Initiation of the First Brittle Fracture and Energy Release
- Dynamic Redistribution of Internal Stresses and Chain
- 3 Momentum Transfer and Ballistic Ejection of Debris

Not all stored energy causes motion and some is lost through different factors.

We qualitatively analyzed the amount of energy loss, with the highest portion attributed to fracture energy waste the energy released and dissipated when the spaghetti breaks in the tube. Then friction & stress waves, and finally other factors such as air resistance and sound make energy loss.

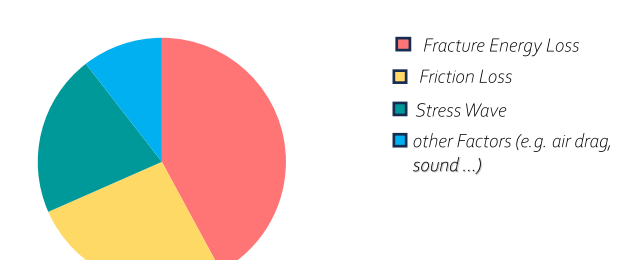


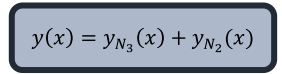
Fig. 6: Energy loss

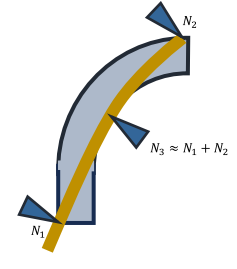
#### 4. Quantitative Analysis

In our theoretical approach, we modeled the spaghetti as an elastic beam, specifically using Euler-Bernoulli beam theory. So the governing static Oiler Bernoulli beam theory is calculated by this formula.

$$EI\frac{d^2y(x)}{dx^2} = M(x)$$

- E = Young's modulu.
- I = Second moment of area
   y(x) = Deflection profile
- M(x) = Bending moment





Because there are 3 loads acting on the spaghetti  $N_i$ ,  $N_2$  form the breaking points and the last one  $N_3$  form end the deflection profile should be superposition of  $N_3$  and  $N_2$  which get the equation y(x).

To analyze the deflection profile of the spaghetti inside the bent tube under an applied force, the beam was divided into two regions: where a is the position of the applied force P, and L is the total length of the spaghetti. For each region, we use the Euler-Bernoulli beam theory to derive the deflection equations. In the first segment the deflection is given by this formula:

is given by this formula:  

$$0 \le x \le a: \ y_P(x) = \frac{Px^2}{6EI}(3a - x)$$

In the second segment the deflection follows by this formula:

$$a \le x \le L: \ y_P(x) = \frac{Pa^2}{6EI}(3x - a)$$

P: applied force 
$$\left(\frac{kg.m}{s^2}\right)$$
  
L: lenght(m) | E: Young's modulus  $\left(\frac{N}{m^2}\right)$   
 $I = second\ moment\ of\ area(m^4)$ 

Here, we further analyze the deformation of the spaghetti due to the applied load N using beam mechanics.

The diagram illustrates the deflection shape more clearly, showing the response of the spaghetti as it bends along the curved section of the tube. It yields the deflection of spaghetti.

For the **upward** load N at x = b:

$$0 \le x \le L: \ y_N(x) = \bigoplus_{\substack{\downarrow \\ \text{(Upward force)}}} \frac{x}{6EI} (3L - x)$$

Thus this is the overarching equation that will determine the deflection profile of the spaghetti in this phenomenon. We consider both the axial load and bending force which form the deflection profile that stores energy. At maximum curvature, the spaghetti is on the edge of fracturing on the location of X.

$$y(x) = y(x)_{P} + y(x)_{N}$$

$$y(x) = \begin{cases} \frac{Px^{2}}{6EI}(3a - x) - \frac{Nx^{2}}{6EI}(3b - x) & 0 \le x \le a \\ \frac{Pa^{2}}{6EI}(3x - a) - \frac{Nx^{2}}{6EI}(3b - x) & a \le x \le L \end{cases}$$

Euler Bernoulli beam theory is applied to calculate the potential energy stored in the spaghetti.

By applying the principles of energy conservation, we calculated the theoretical exit velocity of the spaghetti

debris. The stored elastic energy at the breaking point is rapidly converted into kinetic energy, propelling the fragments outward. This conversion is key to explaining the high-speed ejection.  $\eta$  is our experimentally determined efficiency factor. We derived expressions for the bending energy, and by applying energy conservation, we estimated the velocity at which the debris would be ejected.

Elastic Potential Energy of a Euler Bernoulli Beam:

$$\begin{split} U_{elastic} &= \frac{1}{2} \int\limits_{0}^{L} EI[y'']^2 dx \\ U_{elastic} &= \frac{1}{2} \left[ \int_{0}^{a} EI[y'']^2 dx + \int_{a}^{b} EI[y'']^2 dx + \int_{b}^{L} EI[y'']^2 dx \right] \\ \frac{1}{2} m v^2 &= \eta U_{elastic} \\ 0 &< \eta < 1 \longrightarrow \text{Experimentally we found } \eta \approx 0.3 \end{split}$$

L: lenght(m) | E: Young's modulus  $\left(\frac{N}{m^2}\right)$  |  $I = second moment of area(m^4)$  | m: mass of the projectile(kg) | v: velocity of projectile( $\frac{m}{s}$ )

One specific model we used is the cantilever beam, where one end is fixed and a load is applied to the other. This helps approximate the spaghetti's behavior inside a fixed-length curved tube.

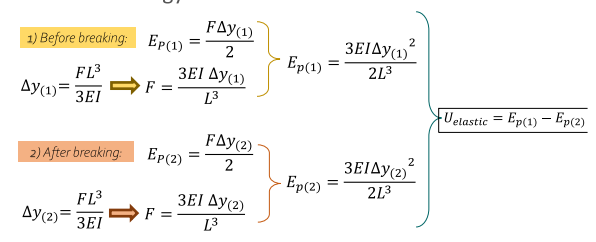
The curvature introduces bending moments, and we calculated the maximum stress at different sections to find potential breaking points.

Elastic Potential Energy  $\Delta y = \frac{FL^3}{3EI}$  Second Moment of Area  $I = \frac{\pi}{2}r^4$   $I = \frac{\pi}{2}r^4$   $I = \frac{\pi}{2} \text{Polymward Force}$  I = Initial Length E = Young's Modulus I = Second moment of area  $\Delta y = \text{Definition}$ 

To calculate the output velocity, we need the amount of energy stored in the spaghetti. To determine this, we used the formula for a cantilever beam. We observed that before and after the spaghetti breaks and a piece is ejected, it bends. By calculating the amount of bending before and after the break, we can estimate the output energy.

By modifying the cantilever beam formula, we arrive at this equation, then calculate the stored energy in the first and second states. Finally, we calculate the total stored energy using this approach.

Potential Energy Calculation



### 5. Experiment Verification & Parameter Analysis

Bending angle of the tube is one of the parameters which affects the speed of ejection. The chart shows the velocity as a function of the tube's bending angle. As it is seen, the output velocity increases with the increase in the bending angle. Additionally, one of the limitations of this experiment is the low bending angle. For example, in the case of spaghetti with a diameter of 1.5 mm, if the bending angle of the tube is less than 35 degrees, the spaghetti does

not break but only bends. This limit varies for different types of spaghetti.

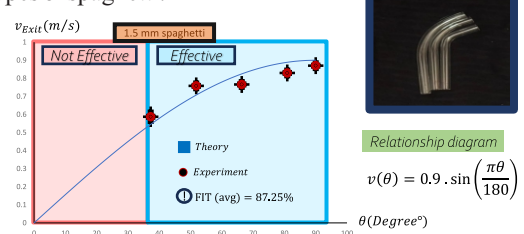


Fig.7: Bending angle of the tube

We also looked at the tube material. More friction increases confinement, enhancing stress buildup and changing where breaks occur. By analyzing our experiment and tests we plot this graph for 3 different materials of the tube (Fig. 8).

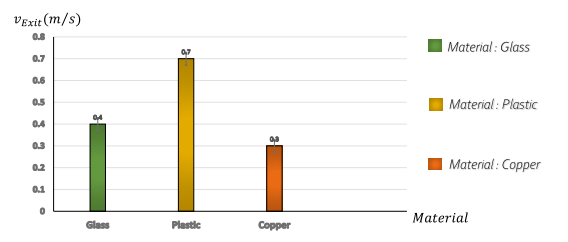


Fig. 8: Tube Materials

Then we analyzed the effect of the tube outer diameter in this phenomenon. The chart follows an exponential decay (Fig. 9).

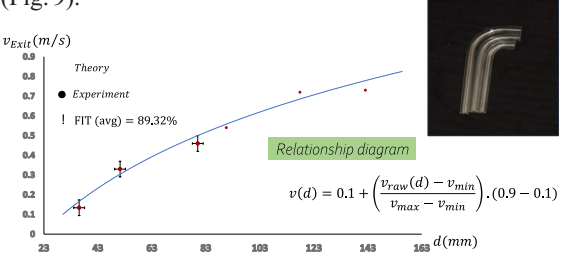


Fig. 9: Tube outer diameter

To apply beam theory accurately, we measured spaghetti's Young's modulus via tensile tests. We also calculated the second moment of area for its cylindrical shape (Fig. 10).

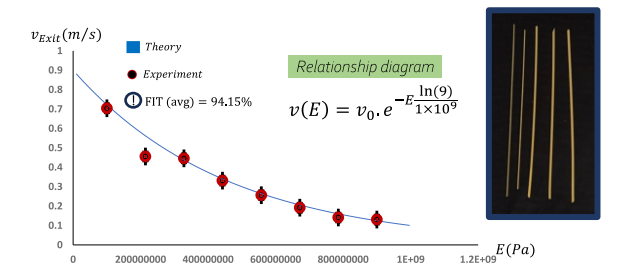


Fig. 10: Young Modules of spaghetti

The Young's modulus of spaghetti was measured to quantify its stiffness. Young's modulus, denoted by E, is a fundamental material property that relates stress and strain. To find the modulus of elasticity and the moment of area for spaghetti, we use the cantilever beam formula. By simply knowing the applied force and the amount of

deformation, we can calculate the modulus of elasticity and the moment of area. To do this, we fix one end of the spaghetti as a cantilever and apply a force vertically upward at the other end using a force gauge, causing it to bend and deform.

$$E = \frac{FL^3}{3Iy} \qquad I = \frac{\pi}{2}r^4$$

- F = Downward Force
- I= Initial Length of the free part of the spaghett
- E = Young's Modulus of the spaghetti
- I = second moment of area
- y= Deflection of the spaghetti
- b= width of the spaghetti
- h= thickness of the spaghett



Then the graph is plotted which its gives the value of E and I(E) = 11

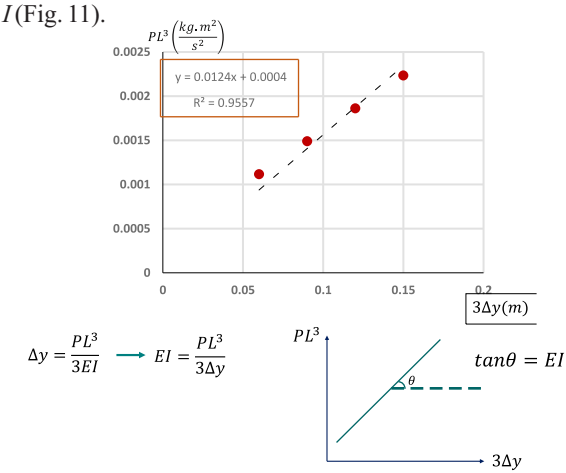


Fig. 11: Measuring Young's Modulus and second moment of area

The spaghetti diameter was changed too. Thicker spaghetti stores more energy and may require more force to break (Fig. 12).

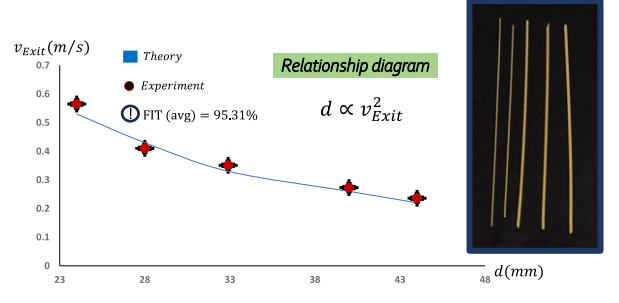


Fig. 12: Diameter of spaghetti

#### 6. Conclusion

By using the cantilever beams formula the potential energy stored in the spaghetti was calculated before and after fracture. Then by applying the principle of energy conservation, the exit velocity of the fragments was measured. Finally, the verification between theory and experiments was done and the effects of key parameters were examined such as: Bending angle of the tube, Tube outer diameter, Tube inner diameter, Tube material, Young modulus of spaghetti and Diameter of spaghetti.

#### References

[1] Strogatz, S. H. Nonlinear Dynamics and Chaos: With Applications to Physics, Biology, Chemistry, and

- Engineering. Westview Press, 2015.
- [2] Moon, F. C., & Holmes, P. J. (1979). A magnetoelastic strange attractor. Journal of Sound and Vibration, 65(2), 275–296.
- [3] Motter, A. E., Gruiz, M., Károlyi, G., & Tél, T. (2003). Doubly Transient Chaos: Generic Form of Chaos in Autonomous Dissipative Systems. Physical Review Letters, 111, 194101.
- [4] Moon, F. C., & Holmes, P. J. (1979). A magnetoelastic strange attractor. Journal of Sound and Vibration, 65(2), 275–296

# THE EFFECT OF DIFFERENT SALTS ON ONION CELL STRUCTURE

Saina Nikmehr, Farzanegan 1 School, nik2000@gmail.com

ABSTRACT

ARTICLE INFO

Participated in PYNT 2020

Advisors: Rozhin salmani ,Hedieh pourghasem

Accepted in country selection by Ariaian Young

Innovative Minds Institute , AYIMI

http://www.ayimi.org,info@ayimi.org

he main structure of the onion cell consists of a cell wall which, with its strength and cellulose structure, forms a polygonal cell, the cell membrane, the cytoplasm which contains organelles, chloroplasts and central vacuole, which is the largest part of the cell and includes water and food. In this paper, we intend to compare the effect of different salts on onion cell structure based on their concentration by comparing the cell's situation before and after the experiment. Finally, the purpose of this research, is to study the factors related to the amount of cell osmosis.

Key Words: Salt,, Onion Cell, Osmotic Pressure, Plasmolysis

# 1. Introduction

Have you ever thought about the effect of various salts on the onion cell? for investigating and answering the question raised in this study first, we remove the purple epidermis of the onion cell and then take a picture of its previous state under the microscope, in the Next step, we use a dropper, and then pour a few drops of the salt solution over the sample and after that by taking some pictures at different time lapses, the changes would be recorded in the images.

Walter Stiles and Ingvar Jorgensen, who also published an article in 1918 entitled "On the Relation of Plasmolysis to the Shrinkage of Plant Tissue in Salt Solutions" were the first researchers who examined the relationship between cellular plasmolysis and shrinkage of plant tissue. A few years after Nobur, Kamiya, and Masashi Tazawa in 1955 published an article entitled "Studies on Water Permeability of a Single Plant Cell by Means of Transcellular Osmosis", which in that time this paper developed a new method for the measurement of permeability of the cell to water and other research by different scientists.

But up to now, the factors affecting cellular osmosis have not been discussed precisely, and we intend to investigate this subject more precisely in this article. Other reasons include inappropriate technology, inaccuracy in hygiene conditions, the onion product packaging and storage conditions do not allow the proper use of this product. Osmotic dehydration is a storage method that delivers the highest possible quality by transporting water out of the foodstuff tissue, and by determining the factors related to the amount of cell osmosis, the amount of product osmosis can be controlled so then by using osmotic dehydration, the characteristics quality of the processed product can be improved.

Various factors such as temperature, concentration of osmotic solutions, proportion of sample to solution, time and physical and chemical properties of an onion are effective in the osmotic process.

# 2. Research Method

For doing the experiments, first, we remove the purple epidermis of the onion cell and then take a picture of its previous state under the microscope, in the Next step, we use a dropper, and then pour a few drops of the salt solution over the sample and after that by taking some pictures the changes would be recorded.

We used purple onions to study the effect of different salts on the structure of the onion cell because it contains the anthocyanins pigment molecule which is purple and make the visibility of the vacuole better under the microscope. We used four types of salts, NaCl, NaBr, KBr and KCl to study the effect of salts because, these are soluble in water and also the number of particles in each molecule of those salts are equal with each other.

#### 3. Experiments

Our experiments are divided into three parts:

Part one: In this section, the variable is type of salt, we used NaCl, NaBr, KBr and KCl solutions with the same mass concentrations (5 percent). We recorded the vacuole changes by taking pictures in this section for all of our salt solutions after 4 minutes we dropped the solution on the onion cell.

Part two: In this section, the variable is type of salt and we used NaCl, NaBr, KBr and KCl solutions with the same molar concentrations (1 molar). We recorded the vacuole changes in this section for all steps in three time lapses of 3, 4 and 5 minutes after we dropped the solution on the onion cell.

Part three: In this section, the variable is the salt concentration for which we used sodium chloride. We used different concentrations of 0.5%, 1%, 2%, 5% and 10%. We recorded vacuole changes in this section for all steps in three time lapses of 3,4 and 5 minutes after we dropped the solution on the onion cell.

Finally, in this paper, the approximate range of hypertonic, isotonic and hypotonic sodium chloride solutions equal with the red onion cell are measured and also the effect of different type of salts on the amount of plant cell osmosis is also examined.

# 4. The Results

The results of the first part of the experiment:

The diagram shows the plasma membrane length changes before and after the experiment. It should be noted that the cell wall length has not changed (Fig. 1).

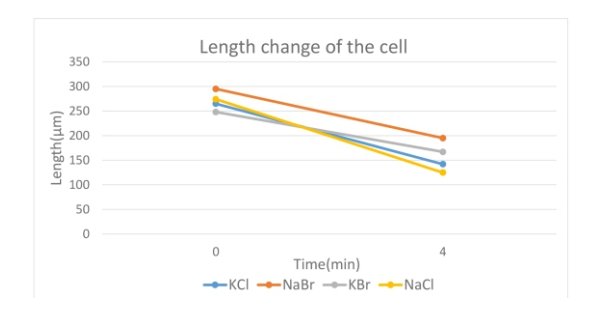


Fig. 1: Changes of the cell wall length Vs time

According to the figure (1), the cell length has decreased in all salt solutions because of the cell plasmolysis which means, the water has exited from the cell. Comparison of the amount of plasmolysis in the salt solutions:

KBr solution<NaBr solution<KCl solution<NaCl solution

According to the table and figure (1), salts with lower molar mass, have higher plasmolysis

Table 1: The molar mass of the salts

NaCl	KBr	NaBr	ксі
58.44 g/mol	119.002 g/mol	102.894 g/mol	74.551 g/mol

The pictures of the cells after the experiment are in figure (2).



Fig. 2: Different salts on onion cells after 4 Min.

The plasma membrane length changes before and after the experiment are in figure (3). It should be noted that the cell wall length has not changed.

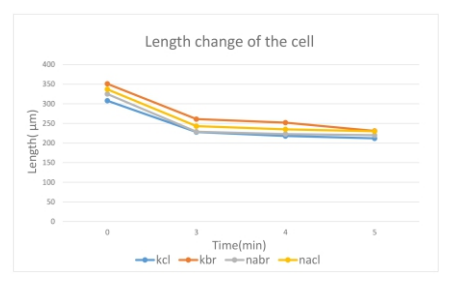


Fig. 3: Changes of the plasma membrane length Vs time

The plasma membrane width changes before and after the experiment are in figure (4). It should be noted that the cell wall length has not changed.

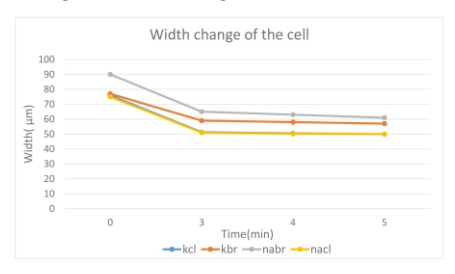


Fig. 4: Changes of the plasma membrane width Vs time

According to figure (3), the trend for all salt solutions was decreasing, so the cell length was reduced, because of the plasmolysis. Also the decreasing trend of cell length for almost all salt solutions has been the same, which can tell us that the type of salt was not effective in the amount of osmosis.

According to figure (4), the trend for all salt solutions was decreasing, so the cell width decreased from its previous state because of the plasmolysis. Also the decreasing process of cell width for almost all the salt solutions has been the same. As a result, the type of salt was not effective.

The pictures of the cells before and after the 5 minutes are in figure (5).

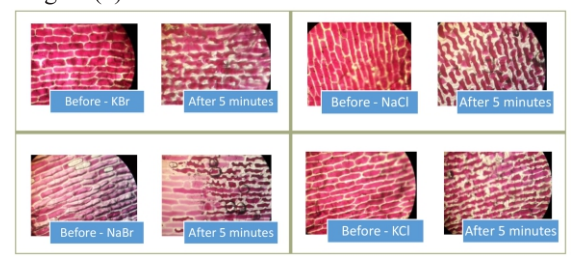
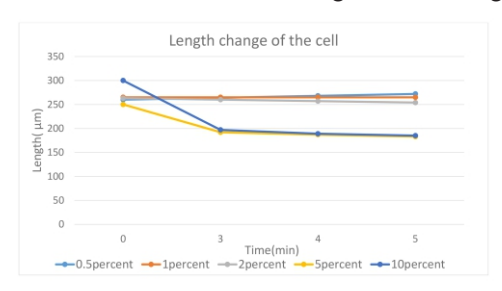


Fig. 5: Different salts on onion cells after 5 Min.

The results of the third part of the experiment:

The plasma membrane length changes before and after the experiment (Fig. 6) (by different percentage of salts). It should be noted that the cell wall length has not changed.



**Fig. 6:** The plasma membrane length Vs time in different percentage of salts

The plasma membrane width changes before and after the experiment (Fig. 7) (by different percentage of salts). It should be noted that the cell wall length has not changed.

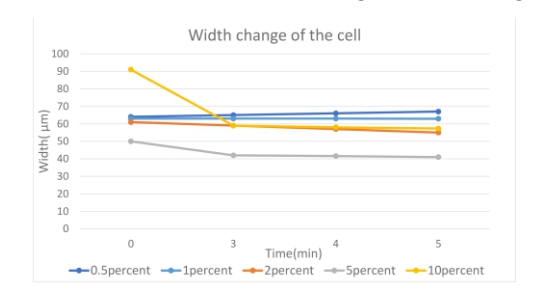


**Fig. 7:** The plasma membrane widthVs time in different percentage of salts

According to these figures, in 0.5 percent NaCl solution, a small amount of turgency has occurred, meaning that water has entered the cell, thereby the length and width of the cell has increased slightly. Also, in 1 percent NaCl solution, the length and width of the cell has not changed. In 2 percent NaCl solution, the width and length of the cell has decreased a little so a small amount of plasmolysis occurred, meaning that the water was exited from the cell.

In 5 percent NaCl solution, Plasmolysis occurred, meaning that water was exited from the cell, thereby cell length and width has reduced. In10 percent NaCl solution, a lot of plasmolysis has occurred, which means that the water was exited from the cell and the length and width of the cell has decreased Sharply (Fig. 8).

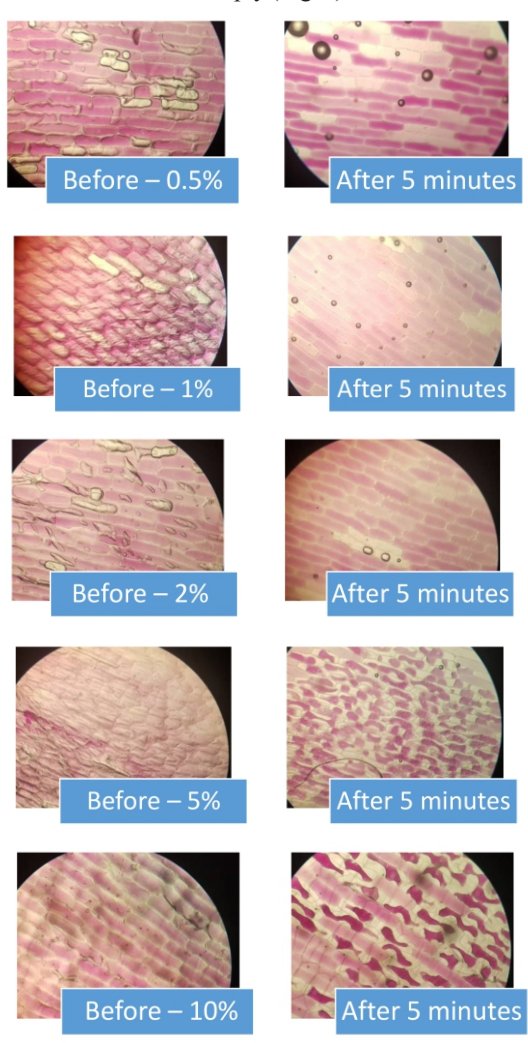


Fig. 8: Different changes in onion cells by different percentage of

#### 5 Discussion and Analysis

The cause of cell plasmolysis:

The concentration of the solutes outside the cell is higher than the inside of the cell, and this is true for all the salt solutions we have used. This type of solutions is called hypertonic solutions. As a result, the osmotic pressure of the salt solution is higher than the osmotic pressure inside of the cell.

Osmosis occurs when two solutions, containing different concentrations of solute, are separated by a selectively permeable membrane. Solvent molecules pass preferentially through the membrane from the low-concentration solution to the solution with higher solute concentration. The transfer of solvent molecules will continue until equilibrium is attained so the water molecules will move from the cell to the outside of it. Both salt ions used in each of the four salts are large in size so they can't pass through the cell membrane and also the cell membrane has selective permeability because it is a semipermeable membrane and the cell membrane doesn't let the ions to pass, in fact the system of transportation in

our experiments is osmosis because every salt ion doesn't have the necessary conditions to pass through the cell membrane by other transportation systems. so the osmosis occurs and Osmosis only permits water to pass and for balancing the pressure on both sides of the membrane, the water moves from inside of the cell to outside of it so, the cell would shrink.

The largest part of the cell is vacuole where most of the cell's water is stored so most of the water would exit from this organelle and the shrinkage of vacuole affects the shape of cytoplasm so the size of cytoplasm will be lower with the size of vacuole but the size of cell wall wouldn't change (Fig. 9).



Fig. 9: The shrinkage of vacuole affects the shape of cytoplasm

Analysis of the results of the first part of the experiments: As mentioned cells placed in salt solutions with lower molar mass had more plasmolysis. This results are because in this section the mass concentrations of our solutions are equal so the molar concentrations of them are different. The mass of one mol of those salts which have less molar mass, is lower. So in the same mass concentrations the salts with lower molar mass have higher molar concentration. As a result, the number of salt molecules in those solutions are higher so they attract more water molecules and because of that the plasmolysis in those solutions would be higher too.

Finally, the aim of this project is to understand the effect of the type of salts on the amount of osmosis, so this type of experiment isn't correct because, the molar concentrations aren't equal so it makes experimental errors. In the next section, the effect of different salts is investigated.

Analysis of the results of the second part of the experiments:

According to this part, the downward trend of cell length and width in all four types of salts was close to each other. So from this section it can be concluded that the type of salt is not effective in the amount of cell osmosis. For proving this part, the van't hoff's equation is needed. With this law the osmotic pressure of a solution can be measured.

The osmotic pressure of a solution is the minimum amount of pressure needed to prevent water from flowing into it across a semipermeable membrane.

The van't hoff equation:

# Π=iMRT

 $\Pi$  is the osmotic pressure in atm

I = van 't Hoff factor of the solute

M = molar concentration in mol/L

 $R = universal gas constant = 0.08206 L \cdot atm/mol \cdot K$ 

T = absolute temperature in K

Osmotic pressure obeys a form of the ideal gas law and can be calculated provided you know the concentration of the solution in molar and the temperature in kelvin because other factors are constant. In this part of the experiments, the molar concentrations and the

the molar concentrations and the temperature of the solutions are equal with each other and the other factors are constant. therefore, the osmotic pressure of the solutions is equal with each other. Thus, the amount of pressure required to prevent the water from exiting the cell is the same for all of them, therefore the amount of water would exit from the cell for all four types of salts are equal, so the amount of plasmolysis would be equal too and because of that their downward trend on the chart is almost similar to each other.

Analysis of the results of the third part of the experiments:

The purpose of this section was to show that the effect of salt on the onion cell is not just plasmolysis and the shrinkage of the cell, and various effects can be observed by changing the concentration of the salts in the solutions. The effects of it are divided into three cases, depending on the concentration of solution relative to the concentration of solutes in the cell:

Case One: In this case, the concentration of solution is higher than the concentration of the solutes in the cell, so the water exits from the cell to the outside of it therefore, the cell shrinks. This type of solution is called hypertonic solution and this shape of cell is called plasmolysis.

Case Two: In this case, the concentration of solution is lower than the concentration of the solutes in the cell, so the water enters into the cell therefore, the cell swells. This type of solution is called hypotonic solution and this shape of cell is called cytolysis.

Case Three: In this case, the concentration of solution is equal with the concentration of the solutes in the cell, so the shape of the cell wouldn't change. This type of solution is called isotonic solution.

According to the figures in this section the shape of the cell after the experiment was like this:

0.5 percent solution	Turgid
1percent solution	No change
2 percent solution	little plasmolysis
5 percent solution	plasmolysis
10 percent solution	high plasmolysis

Another thing we can conclude from this part is that by increasing the concentration of the salt in the solution, the molar concentration would be higher so the plasmolysis would be higher too (Fig. 10).

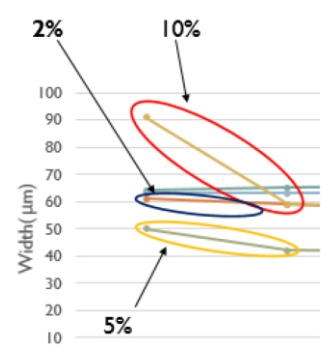


Fig. 10: The molar concentration would be higher so the plasmolysis would be higher too

The approximate range of hypertonic, isotonic and hypotonic sodium chloride solutions are equal with the red onion cell we experimented (Table 2).

**Table 2:** The approximate range of hypertonic, isotonic and hypotonic sodium chloride solutions

	Lower than 0.5% or equal to it	1 percent	Higher than 2 percent
The type of solution	Hypotonic solution	Isotonic solution	Hypertonic solution
cell shape	Cytolysis and turgid	No changes	Plasmolysis and shrinkage

#### References

- [1] Regulation of Water in Plant Cells, Richard V. Kowles, May 2010
- [2] The Movement of water molecules in response to the solute concentration, Baken Johannes Lefa,18March 2015
- [3] OSMO-Convective Drying of Onion Slices, Patil M.M., Kalse S.B. and Jain S.K., 28 September 2011
- [4] Salt tolerance in tissue culture of onion (Allium cepa L.), S.A. Bekheet; H.S. Taha and M.E. Sollima, January 2006
- [5] Response of onion to salinity, Sta-Baba, R. & Hachicha, M. & Mansour, Mohsen & Nahdi, H. & Kheder, 2010
- [6] https://www.researchgate.net/publication/ 295989047 Sodium Chloride in Nutrient Solutions
- C

an Affect Onion Growth and Flavor Development

[7] https://www.sid.ir/en/journal/ ViewPaper.aspx?ID=269323

# INVESTIGATION OF LATO LATO OSCILLATION

<sup>a</sup> Arman Ardavani, <sup>b</sup>Atoosa Esmaeili, a) Iranian Cambridge School, <u>arman.ardavani@gmail.com</u>, b) Farzanegan 2 School, atoosaesma992009@gmail.om

#### ABSTRACT

#### ARTICLE INFO

(a) Iran Team Member in AYPT 2025, Austria

Advisors: Amirreza Soheili, Mohammadmahdi Shariatmadar

Accepted by Ariaian Young Innovative

Minds Institute, AYIMI

http://www.ayimi.org,info@ayimi.org

where two balls collide each other and move freely whereas both are attached to the string. In order to get a glimpse into this motion we first go to the initial observation as  $(b) Iran \, Team \, Member \, in \, IYPT \, 2025, Lund \, University, Sweden \, \\ the \, introductory \, phase \, . \, This \, phenomenon \, supposed \, to \, be \, investigated \, as \, the \, periodic \, motion \, that \, in the introductory \, phase \, . \, This \, phenomenon \, supposed \, to \, be \, investigated \, as \, the \, periodic \, motion \, that \, in the introductory \, phase \, . \, This \, phenomenon \, supposed \, to \, be \, investigated \, as \, the \, periodic \, motion \, that \, in the introductory \, phase \, . \, This \, phenomenon \, supposed \, to \, be \, investigated \, as \, the \, periodic \, motion \, that \, in the introductory \, phase \, . \, This \, phenomenon \, supposed \, to \, be \, investigated \, as \, the \, periodic \, motion \, that \, in the introductory \, phase \, . \, This \, phenomenon \, supposed \, to \, be \, investigated \, as \, the \, periodic \, motion \, that \, in the introductory \, phase \, . \, This \, phenomenon \, supposed \, to \, be \, investigated \, as \, the \, periodic \, motion \, that \, in the introductory \, phase \, . \, This \, phenomenon \, supposed \, to \, be \, investigated \, as \, the \, periodic \, motion \, that \, in the introductory \, phase \, . \, This \, phenomenon \, supposed \, to \, phenomenon \, pheno$ the pendulum acts harmonic or chaotic. When the pivot is oscillated along the vertical direction, the balls start to collide with increasing amplitude and damp after we stop oscillating the pivot . The Key parameters of the phenomenon which have been studied are: period and oscillation range for the pivot, material and length of the strings, Mass and the material of the balls ..

he problem asks us to look at Lato - Lato which is used as a toy in physics education

Keywords: Lato Lato, Oscillation, Damped Motion, Harmonic

#### 1. Introduction

In order to get a glimpse into this motion we first go to the initial observation as the introductory phase.

As problem mentioned we basically took two balls and attached them through a string. By moving the point as the pivot up and down we got to the motion of lato lato.

Two things are happening that are the key components to this issue. The 1st one is internal collision that occur between the balls and the second one is the periodic motion these two balls exhibit after a while.

Now in order to get a glimpse into what was researched about this problem we go to the literature review.

It is found two distinct scenario: Phase 1 and phase 2 which are solved in two approaches.

This phenomenon supposed to be investigated as the periodic motion that the pendulum acts harmonic or chaotic. The Lato-Lato mechanism is based on a cyclic process involving excitation, amplitude growth, and collisions (Fig. 1).



Parametric Excitation(Vertical Oscillation)



Fig. 1: Lato-Lato Mechanism

### 2. Qualitative Analysis

The physics behind this repetitive and rhythmic motion is actually quite complex. It involves forced oscillations, collisions, and energy dissipation.

The motion of Lato-Lato can be described as a forced, damped oscillator. The vertical movement provides a periodic forcing term, while air resistance and internal friction create damping. But the real twist is the repeated inelastic collisions, which act like sharp energy-loss events. These impacts make the system more complex than a regular forced oscillator (Fig. 2).

In ideal circumstances without waste of energy when we oscillate the pivot in vertical direction in a specific constant

range after each collision the distance between the balls would increase (Fig. 3).

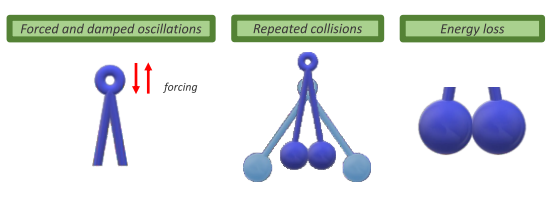


Fig. 2: Phenomenon explanation

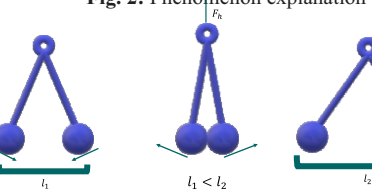


Fig. 3: Increasing the distance between two balls

When the masses are equal, the motion is very regular. Each ball transfers its energy to the other almost perfectly. This results in a rhythmic, repeating motion ideal for sustained Lato-Lato and both balls have equal velocity since the masses are same (Fig. 4).

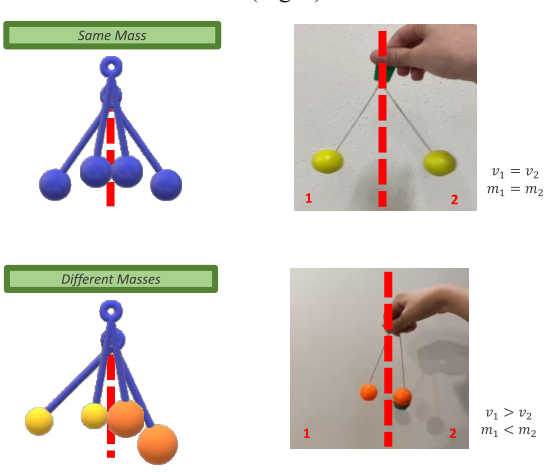


Fig. 4: Equal and different masses

If the two balls have different masses, the outcome of collisions becomes unbalanced. The lighter ball bounces off with more speed, and the motion can become irregular. Here, mass 2 is more than mass1 and it's moving slower. But the collision point is constant, so the energy of both balls is equal.

The motion of Lato-Lato can be divided into two distinct phases. The first phase represents the normal pendulum motion and the second phase represents the condition at which the spheres collide at both  $\theta=0$  and  $\theta=\pi$  rads (Fig. 5).

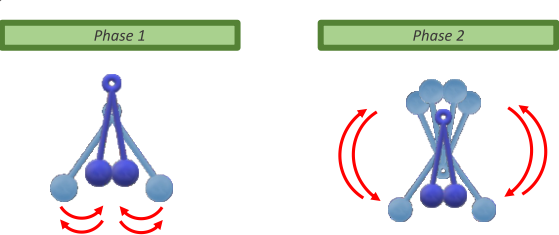


Fig. 5: Phase Alignment

Phase 1: Oscillation Phase

It is when one ball swings like a pendulum and builds up speed due to gravity. Here, the motion is described by damped forced oscillation.

Phase 2: Collision Phase

This is the key moment when the two balls collide at the top of the arc. In this phase, the interaction is modeled as a partially elastic collision meaning not all kinetic energy is conserved due to internal deformations and sound.

This collision determines how energy and momentum are transferred between the balls, setting up the rhythm for the next cycle.

In Lato-Lato, each time the balls collide, some energy is lost. This is because of the coefficient of restitution, or COR, which is a number between 0 and 1 that measures the 'bouncy' of a collision. When COR of the materials used is less than 1 the collisions are not perfectly elastic.

The lower the COR, the more energy is lost in every hit.

# 3. Experiments

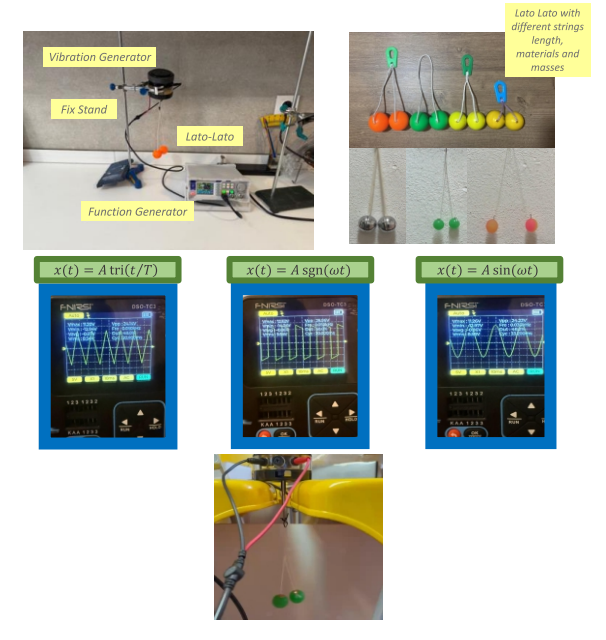


Fig. 6: Experimental setup

The data is collected by the Tracker in this experiment

(Fig. 7).

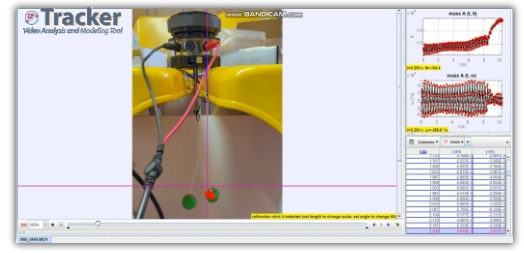
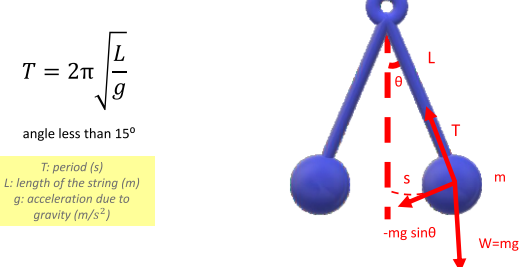


Fig. 7: Tracker to analyze system

# 4. Quantitative Modeling

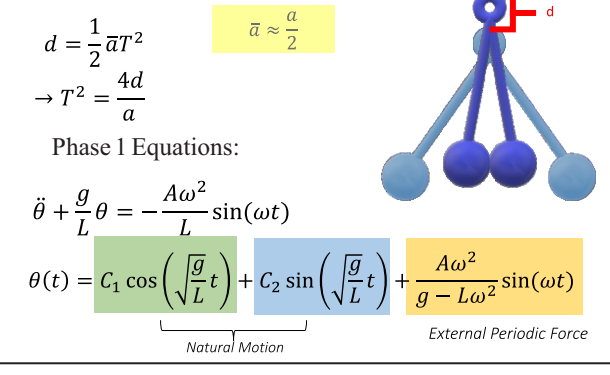
To model the system, we treat each ball as a pendulum. The balls swing due to gravity and the vertical motion of the string's center. This motion acts like a periodic forcing term as follows.



The two balls with the same mass move symmetrically at the same velocity and form a semicircular route with opposing motion directions. the physical essence of the toy lato-lato lies in the law of momentum conservation; the collisions that occur between the plastic spheres are such that  $p_i = p_r$ 

In a normal pendulum, the only acceleration is gravity. But in Lato-Lato, we're shaking the pivot point, meaning the balls feel more than gravity depending on how the pivot moves. In addition to the acceleration of gravity, we introduce another acceleration by oscillating the center of the thread into the Lato Lato. This makes us able to control the behavior of the pendulum. If the hand motion matches the natural frequency, resonance can occur.

In this part of our theoretical model, we analyze the oscillation range specifically, the maximum horizontal displacement, denoted as d, caused by vertical shaking of the pivot. We start with the classical kinematic equation. where  $\bar{a} \approx \frac{a}{2}$  is the average acceleration of the pivot, and T is the oscillation period. Since the pivot accelerates sinusoidally, we approximate the average acceleration over one half-period where a is the peak vertical acceleration of the pivot. This relation helps us estimate required acceleration to reach a specific swing amplitude, or inversely, predict the range from a known acceleration which is very useful when analyzing Lato-Lato behavior under different shaking conditions.



$$C_1 = \theta_0$$
  $C_2 = -\frac{A\omega^2}{g - L\omega^2} \sin(\frac{\omega\pi}{2} \sqrt{\frac{L}{g}})$ 

A: amplitude of forcing

L: length of the string

g: acceleration due to gravity

 $\omega$ : angular frequency

Phase 2 Equations:

$$\ddot{\theta} + \frac{g}{L}\sin\theta = -\frac{A\omega^2}{L}\sin(\omega t)$$

$$\theta(t) = C_1 \cos\left(\sqrt{\frac{g}{L}}t\right) + C_2 \sin\left(\sqrt{\frac{g}{L}}t\right) + \frac{A\omega^2}{g - L\omega^2}\sin(\omega t)$$

External Periodic Force

This is a non-homogeneous second-order linear differential equation, representing a driven (forced) pendulum. describes how the pendulum is not only swinging due to gravity but also being pushed periodically. The external forcing has not yet built up enough energy to make the balls swing all the way up.

The constants  $C_1$  and  $C_2$  depend on the initial conditions. This matches low amplitude forced oscillation.

Now the energy has built up enough due to the forcing. The balls swing over the top and collide both at the bottom and at the top. Nonlinear behavior starts to appear simple harmonic approximations may no longer fully apply. The frequency of the motion may not match the natural frequency anymore; multiple frequencies and more chaotic behavior can emerge. According to The angle  $\theta(t)$  becomes large then small-angle approximation fails and we need to change the equation. To verify the experiment , it is simulated in MATLAB (Fig. 8).

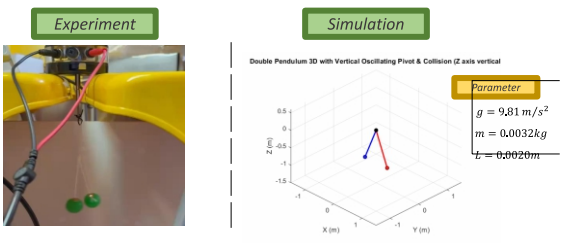


Fig.8: MATLAB Simulation

#### 5. Parameters Analysis

Mass of the balls can affect the motion too. The heavier the balls are, the more energy and momentum is going to be retained, thus the motion is going to continues longer. the lighter the balls are, we are going to lose energy faster and the motion is going to die out quicker (Fig. 9).

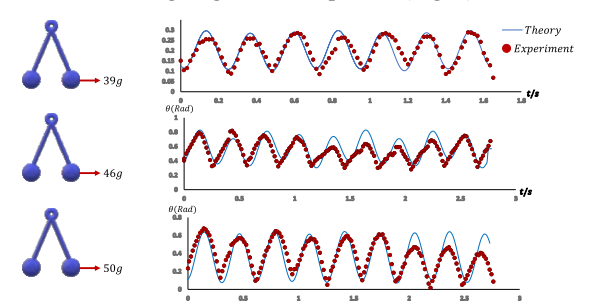


Fig. 9: Comparing experiment and theory in different masses

The other parameter is material which is compared too (Fig 10).

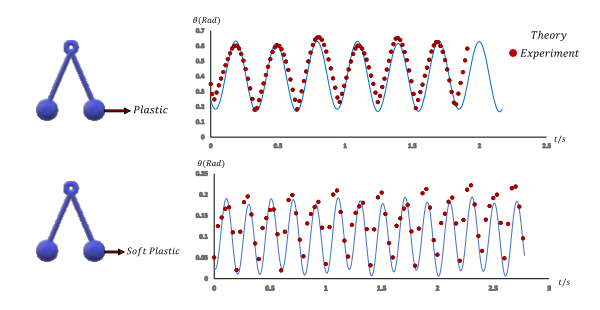


Fig. 10: Different materials

Length of the strings has direct relation with the period. As we increase the length of the pendulum the time that it takes to complete one cycle, increases (Fig. 11).

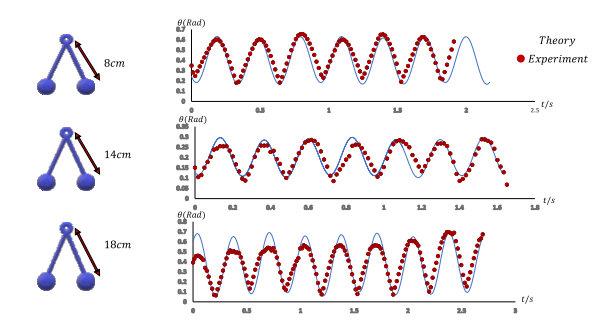


Fig. 11: Different lengths

The relationship between the length of a string (L) and its vibrational frequency (f), shows both theoretical predictions and experimental results. This formula indicates that the frequency decreases exponentially with increasing length, incorporating damping factor (\alpha), gravitational acceleration (g), and other parameters. The graph visually demonstrates that as the length of the string increases, the frequency decreases in a predictable manner (Fig. 12).

$$f(L) \approx \frac{\omega_0}{2\pi} \cdot e^{-\alpha L} = \frac{1}{2\pi} \sqrt{\frac{g}{L}} \cdot e^{-\alpha L}$$

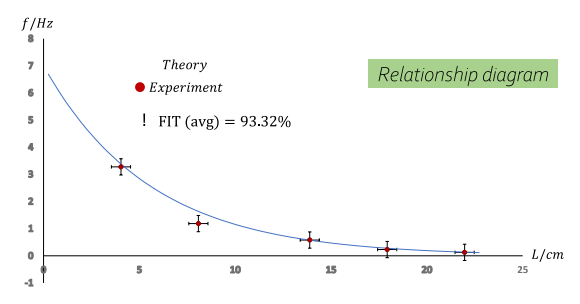


Fig. 12: Frequency Vs Length of String

#### 6. Conclusion

Main Equations were: Forced Equation and Alternating Period Equation

Experiment verification shows:

- High Numerical Accuracy
- Low Experimental Error

Based on the fit between theory and experiment, it can be concluded that in the first setup, the equations used exhibit high numerical accuracy, and the tests performed involve a well-designed setup with minimal error.

# References

- [1] Strogatz, S. H. Nonlinear Dynamics and Chaos: With Applications to Physics, Biology, Chemistry, and Engineering. Westview Press, 2015.
- [2] Moon, F. C., & Holmes, P. J. (1979). A magnetoelastic strange attractor. Journal of Sound and Vibration, 65(2), 275–296.
- [3] Motter, A. E., Gruiz, M., Károlyi, G., & Tél, T. (2003).
  Doubly Transient Chaos: Generic Form of Chaos in
  Autonomous Dissipative Systems. Physical Review
  Letters, 111, 194101.
- [4] Moon, F. C., & Holmes, P. J. (1979). A magnetoelastic strange attractor. Journal of Sound and Vibration, 65(2), 275–296.

# STRANGE MOTION

Aysan Keramat ,Farzanegan2 high school

# ARTICLE INFO

Participated in PYPT 2022

Accepted in country selection by Ariaian Young
Innovative Minds Institute . AYIMI

http://www.ayimi.org,info@ayimi.org

#### ABSTRACT

prinkle small floating particles on the surface of water in a bowl. Bring a strong magnet above and near to the water surface. Explain any observed motion of the particles. The main purpose of the problem is explaining any observed motion of the particles. Experiments on this project show that in paramagnetic fluids, first adsorption and then excretion occur. This phenomenon also occurs if the liquid changes to alcohol, because alcohol is also diamagnetic, so it shows the same behavior as water.

Key Words: Moses Effect, Particles, Diamagnetic, Laser

#### 1. Introduction

Normally there are three types of material in terms of magnetism: ferromagnetic, diamagnetic and paramagnetic. Different liquids and materials exhibit different behaviors in the presence of magnets. Water is one of these materials that shows an interesting behavior in the presence of a magnet because it is one of the diamagnetic materials that is repelled against the magnet. Temperature has no effect on this material because in general, unlike para-magnetic materials, temperature has no effect on diamagnetic materials (Fig.1).

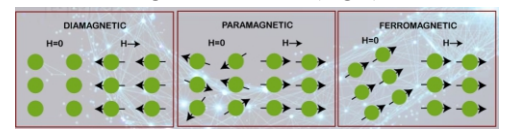


Fig.1: Three types of material in terms of magnetism

Deformation of the surface of a diamagnetic liquid by a magnetic field is called the "Moses Effect". This deformation in water attracts particles and create a current in the direction of the magnetic field. By calculating this deformation, we can also measure the magnetic energy density and the gravitational potential energy density, which according to the law of conservation of energy must be equal.

Due to the behavior of water, which is related to its nonbonding electrons, a Moses effect is created when a magnet is held above or below a container containing a liquid, the liquid will show different magnetic behaviors depending on its type. If it is diamagnetic, a dome is created inward and if it is paramagnetic, it is created upward.

In this question water is diamagnetic so a semicircle is created downward. This phenomenon helps us to justify the behavior of particles (Figs. 2).

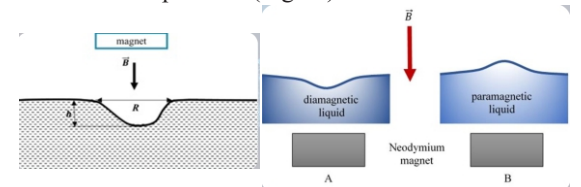


Fig 2. Comparison of phenomena in diamagnetic and paramagnetic fluids and their deformation

Moving and positioning small particles and low liquid volumes are important tasks in miniaturized bio-analytical and biomedical systems, where decreased sample sizes can reduce analysis costs and times.

Water is a diamagnetic fluid because it has no unpaired electrons. Also, the specific locations of water molecules are regular due to the orientation of water molecules in the presence of an induced magnetic field.

Due to the above reasons and the diamagnetic nature of water, it can be said that it is expelled from the magnet.

By measuring the depth of water created, we can calculate the magnetic energy density and the gravitational potential energy density.

#### 2. Experiments and Theory

To measure the water level, we measure the laser to the water level once in the presence of a magnet and once without the presence of a magnet, and measure the maximum water depth by using the height difference created by the reflection of the laser light on the screen (Figs. 3 & 4) (Eqs. 1-8).



Fig. 3. Deformation created in the water surface in the presence of Neodymium magnets

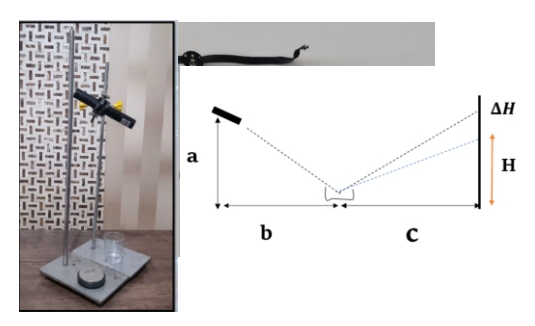


Fig 4. Experimental Setup and Laser test simulation

$$\frac{a+\Delta h}{b} = \frac{?}{c} \rightarrow ? = \frac{c}{h}(a+\Delta h) = H + \Delta H \rightarrow \tag{1}$$

$$\Delta h = \frac{H + \Delta H}{c} \times b - a \to \downarrow \Delta \theta \to \Delta H < 0 \to$$
 (2)

$$\frac{a}{b} = \frac{H}{c} \rightarrow (H + \Delta H)/C = tg(\alpha - 2\Delta\theta)$$
 (3)

$$tg\alpha = \frac{a}{b} \tag{4}$$

The distance from the curtain to the water surface

$$\frac{360mm}{1540mm} \times 7mm = 1.4 \text{ mm}$$
 (6)

Gravitational Potential Energy Density:

$$\mu = \rho g \Delta h \tag{7}$$

$$\mu = 997 \frac{kg}{m^3} \times 9.8 \frac{m}{s^2} \times 0.0014m = 13.7 \text{ kg/ms}^2$$
 (8)

Magnetic Energy Density (Eqs. 9-10):

$$\mu = \frac{B^2}{2\mu_0} \tag{9}$$

$$\frac{0.006^2}{2 \times 1.2566 \times 10^{-6}} = 14.32 \text{ kg/ms}^2$$
 (10)

By the law of conservation of energy, the two energies should be equal.

#### 3. Results and Relevant Parameters

- 1. With the change of fluid, the performance of the system also changes. If the liquid is diamagnetic (residual alcohol that has been tested), it behaves like water and the particles absorb the magnet. If the liquid is para-magnetic, it is first excreted and then absorbed.
- 2. If the particles are denser than water, they will settle and the phenomenon will not be observed. Otherwise, the smaller its size and mass, the faster their movement will increase.
- 3. If the strength of the magnet changes, the stronger the magnet, the clearer and faster the particles move towards the magnet. Also, the strength of the magnet affects the shape of deformation.

#### 4. Conclusions

Due to the diamagnetic nature of water and the effect of Moses, a deformation is created in water and attracts particles, and due to the movement of water molecules and the induction magnet, a current is created.

This phenomenon occurs similarly in diamagnetic fluids. By measuring the maximum depth of water, we can also calculate the magnetic energy density and the gravitational potential energy density, which according to the law of conservation of energy must be approximately equal.

$$13.7 \text{ kg/ms}^2 = 14.32 \text{ kg/ms}^2$$

#### References

- [1] https://www.sciencedirect.com/science/ article/abs/pii/S000186619300636?via%3Dihub
- [2] https://hal.archives-ouvertes.fr/hal-03120755/document

[3] https://www.ias.ac.in/article/fulltext/seca

[4]

https://www.ipho2012.ee/ wp-content/uploads/2012/07/IPhO2012\_ Experimental\_problem.pdf

# **MAGNETIC ASSIST**

Mohammadhossein Ezzati, Valeh School, mhe 8795@gmail.com

#### ABSTRACT

#### ARTICLE INFO

IranTeam Member IYPT 2025, Lund University, Sweden

Advisors: Alireza Noroozshad,

Mohammad Mahdi Shariatmadar

Accepted by Ariaian Young Innovative

Minds Institute, AYIMI

http://www.ayimi.org,info@ayimi.org

ttach one or two magnets to a non-magnetic and non-conductive base such that they attract a magnet suspended from a string. The magnetic pendulum is a striking example of unpredictability in classical physics; a magnetic bob suspended above fixed magnets on a non-magnetic surface exhibits chaotic motion when released. In this study, we investigate the parameters affecting the motion of the moving magnet.

Keywords: Magnetic Pendulum, Non-Magnetic Base, Non-Conductive Base, Chaotic Motion

#### 1. Introduction

The magnetic pendulum is a striking example of unpredictability in classical physics; a magnetic bob suspended above fixed magnets on a non-magnetic surface exhibits chaotic motion when released. In this study, we investigate the parameters affecting the motion of the moving magnet.

Guiding questions are intended as inspiration for beginning our project as:

- How is the magnetic pendulum influenced by the other magnets?
- What forces are at work?
- the instruction and arrangement the magnets should attract each other?
- An arrangement that "supports" the pendulum for example to increase the amplitude beyond the starting amplitude?

In a magnetic pendulum many small rotating magnetic dipoles (on the left,) can create an effective macroscopic field, (on the right). This effective field can exert a torque or lateral force on the moving magnet, leading to rotational or orbit-like motion, which is what we observe experimentally.

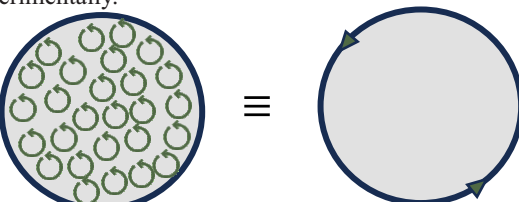


Fig.1: Magnetic dipoles and microscopic field

Three phases should be considered as:

Phase 1. Perturbation Initiation

Phase2. Dynamic Oscillation

Phase3. Equilibrium Stabilization

Now suppose the pendulum consists of a magnet suspended from a string. The plane under the pendulum contains a distribution of like magnets which, based on their number and placement, should affect the dynamics of the pendulum.

Here again external forces are;

Magnetic Force, Drag Force, Gravitational Force and String Tension Force (Fig. 2).

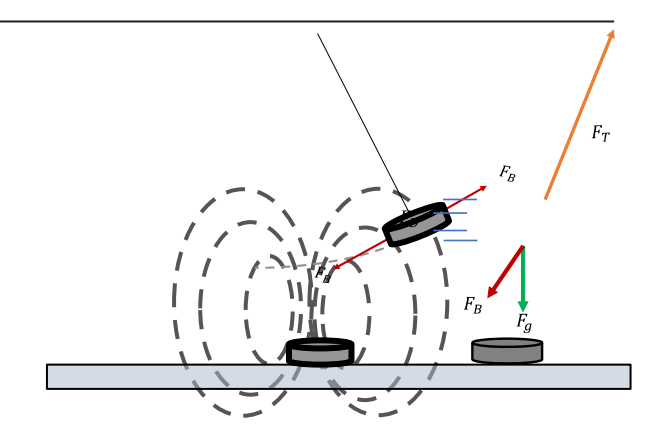


Fig.2: External Forces

#### 2. Quantitative Analysis

In this setup, the magnetic field is generated by permanent magnets fixed on a non-magnetic base. The field depends on the shape, size, and orientation of the magnets, as well as their distance from the suspended magnet.

Magnetic Field:

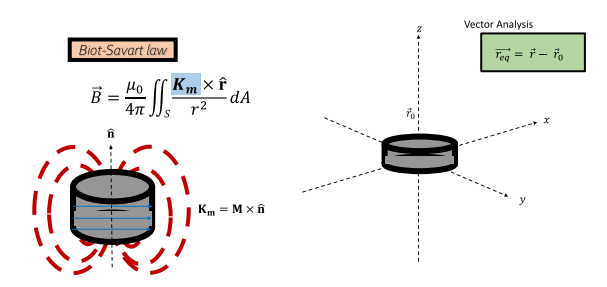


Fig.3: Magnetic Field

The source of the field is the internal magnetic structure of the materials, which creates a specific pattern in space. This field interacts with the suspended magnet and causes it to move, oscillate, or stabilize depending on its position and initial motion.

$$\mathbf{m} = \iiint M \, dV$$
 Dipole Characterization

Dipole Maanet

$$\vec{B} = \frac{\mu_0}{4\pi} \frac{1}{r^3} [3(\vec{m}.\vec{r_{eq}})\hat{r} - \vec{m}]$$

Lorentz Force

$$\vec{F}_{mag} = \iint_{S} \vec{\mathbf{K}}_{\mathbf{m}} \, dS \, \times \vec{B}$$

The magnetic field of a dipole depends on its direction and the position of the observation point.

$$m_r = \mathbf{m} \cdot \hat{\mathbf{r}} = m_x \sin \theta \cos \phi + m_y \sin \theta \sin \phi + m_z \cos \theta$$

$$B_r = \frac{\mu_0}{4\pi} \frac{1}{r^3} [2(m_x \sin\theta \cos\phi m_y \sin\theta \sin\phi + m_z \cos\theta)]$$

$$B_\theta = \frac{\mu_0}{4\pi} \frac{1}{r^3} [m_x \cos\theta \cos\phi + m_y \cos\theta \sin\phi - m_z \sin\theta]$$

$$B_\phi = \frac{\mu_0}{4\pi} \frac{1}{r^3} [-m_x \sin\phi + m_y \cos\phi]$$

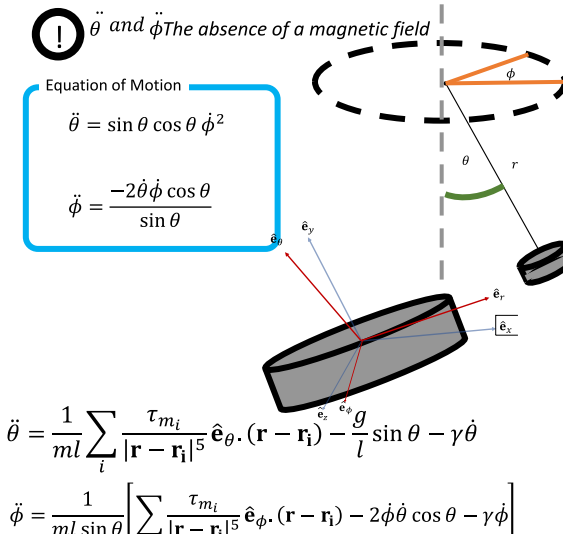
The magnetic force acting on the magnet is calculated by integrating the interaction between the surface magnetization and the magnetic field. This interaction varies across the surface depending on direction and local field strength. The total force is obtained by summing contributions from all surface elements in spherical coordinates.

This result helps explain how the suspended magnet is pulled or pushed depending on its orientation and position.

spherical coordinates

$$r \qquad \theta \qquad \phi \qquad \qquad \mathbf{B} = \mathbf{B_r}\hat{\mathbf{r}} + \mathbf{B_\theta}\hat{\mathbf{\theta}} + \mathbf{B_\phi}\hat{\mathbf{\Phi}}$$
 
$$\vec{F}_{mag} = \iint_S R^2 \sin\theta \, d\theta \, d\phi \begin{bmatrix} K_\theta B_\phi - K_\phi B_\theta \\ K_\phi B_r - K_r B_\phi \\ K_r B_\theta - K_\theta B_r \end{bmatrix}$$

The equations describe how the magnet swings on a spherical path, with  $\theta$  and  $\phi$  influencing each other. Their coupling reflects the complex angular dynamics of the motion.



$$\ddot{\phi} = \frac{1}{ml\sin\theta} \left[ \sum_{i} \frac{\tau_{m_i}}{|\mathbf{r} - \mathbf{r_i}|^5} \hat{\mathbf{e}}_{\phi} \cdot (\mathbf{r} - \mathbf{r_i}) - 2\dot{\phi}\dot{\theta}\cos\theta - \gamma\dot{\phi} \right]$$

Gravitational Force:

$$\ddot{\theta}_g = \frac{-g}{l}\sin\theta$$

String Tension Force:

$$\ddot{\theta}_T = \frac{g}{l}\sin(\theta) - \frac{1}{l}\cos(\theta)\dot{\theta}^2\phi$$

$$\ddot{\phi}_T = -2\cot(\theta)\dot{\theta}\dot{\phi}$$

Drag Force:

$$F_{\theta_D} = -mrC_d \frac{\ddot{\theta}}{\dot{\theta}}$$

$$F_{\phi_D} = -mrC_d \sin \frac{\ddot{\phi}}{\dot{\phi}}$$

These expressions calculate the distance between the suspended magnet and the fixed base magnets as a function of the angle  $\theta$  (Fig. 4).

As the magnet swings, both the vertical and horizontal components change, affecting the magnetic.

$$r_{\theta} = \sqrt{(l\sin\theta)^2 + h_{\theta}^2}$$

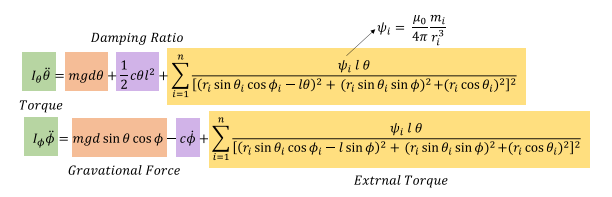
$$h_{\theta} = d + l(1 - \cos\theta)$$

$$F_{\theta}$$

$$F_{\theta}$$

Fig. 4: Applied forces during motion

We considered the moment of inertia of the object as rigid. The sum of the torques are:



$$I_{ heta}\ddot{ heta},I_{\phi}\ddot{\phi}=\sum au_i= au_{Magnet}+ au_{Gravity}+ au_{Damping}$$
 Moment of Inertia 
$$I_{ heta}=ml^2$$
 
$$I_{\phi}=ml^2\sin^2{ heta}$$

m = mass of magnet

 $l = length \ of \ string$ 

c = damping coefficient

d = distance between tow top & down magnet

 $\psi_i$  = The influence coefficient on the magnetic field

The plotted graph is based on the equations of motion. Azimuth and zenith angles versus time are plotted from the theory. Then using the position of the pendulum, we rewrote the equations and determined the angle formed by the magnet.

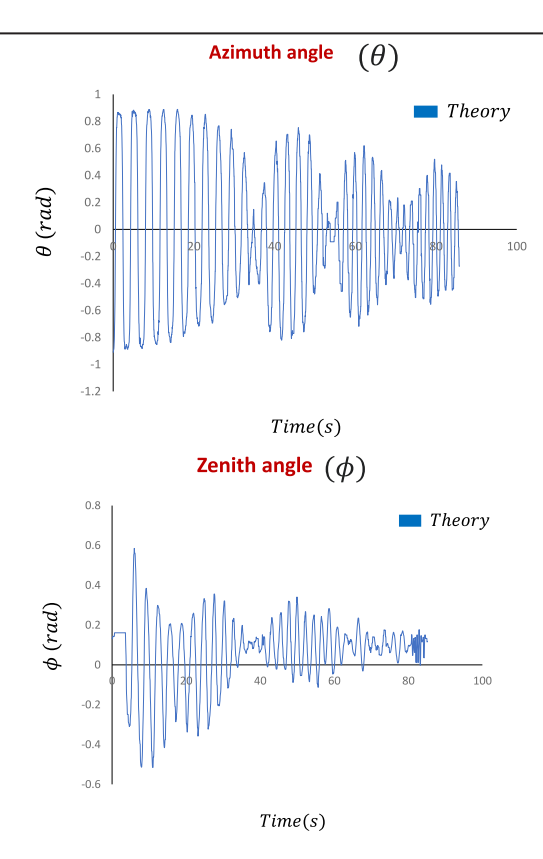
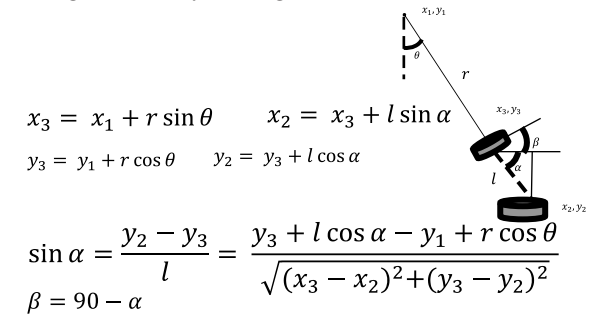


Fig. 5: Two different azimuth and zenith angles versus time

Dynamic Oscillation and the equations to determined the angle formed by the magnet as follows:



The chart shows the oscillations of the damped system, by the gradual decrease in amplitude over time (Fig. 6).

The stable oscillation frequency despite the decreasing amplitude suggests a constant resistive force and The alignment with the analytical model strengthens the results' validity and the dynamic model's accuracy.

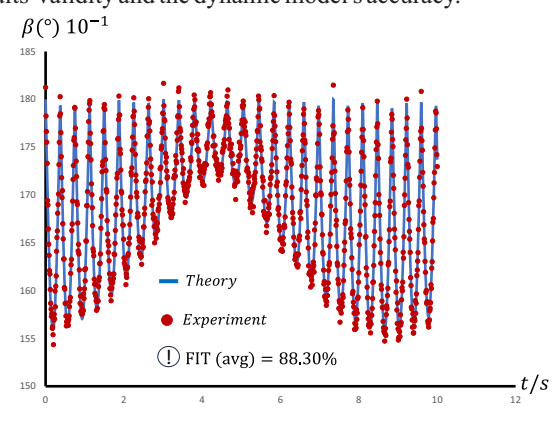


Fig. 6: The oscillation of the damped system

### 3. Experiment & Results

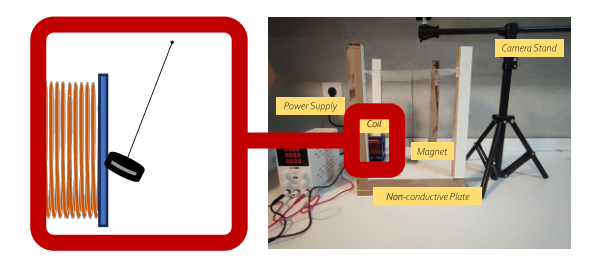


Fig. 7: Experimental setup

A magnet is connected to a coil, and upon deactivating the coil, the magnet is released and coil rapidly moves away. The swinging is seen from top an side views (Fig. 8).





Fig. 8: Swinging of the magnet from top and side views

The experimental setup diagram shows exact places of each items (Fig. 9).

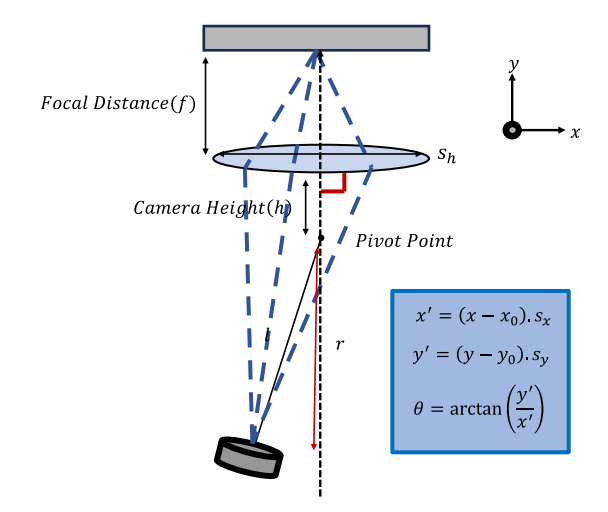


Fig. 9: Schematic of each item

The magnetic field is measured by using a Hall sensor at various angles and distances and damping Coefficient is calculated based on the Logarithmic Decay of Maximum Angular Displacement Over Time".

> Distance of the pendulum from the pivot point in the image plane

$$r = \sqrt{\Delta x^2 + \Delta y^2}$$

> Converting Pixel Coordinates to Real-World Scale

$$d = \frac{r.s_h}{f.p_w}$$

#### > Horizontal Angle of the Pendulum Relative to the Vertical Axis

$$\theta = \arctan\left(\frac{d}{\sqrt{l^2 - d^2}}\right) + \arctan\left(\frac{d}{h}\right)$$

# ✓ Correcting for Perspective Distortion

$$\theta = \arctan\left(\frac{r.s_h}{f.p_w.\sqrt{l^2 - d^2}}\right) + \arctan\left(\frac{r}{h}\right)$$

The initial experiments are tracked by tracker.

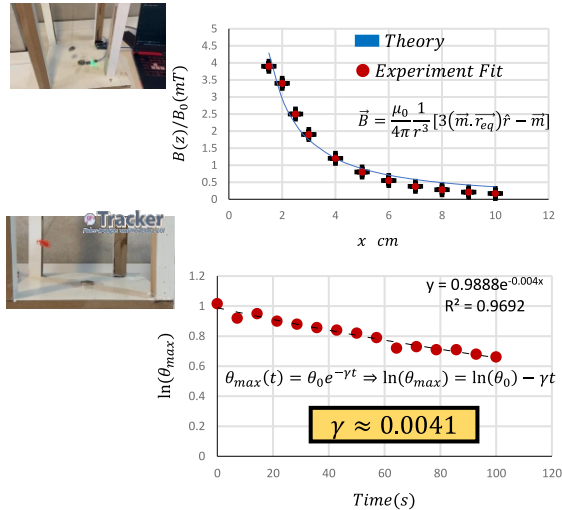


Fig. 10: Tracking the pendulum

The phases are identified based on the amplitude of oscillation (Fig. 11).

Given the low damping coefficient, the system does not come to rest within the observed time interval; however, a gradual decrease in amplitude is evident.

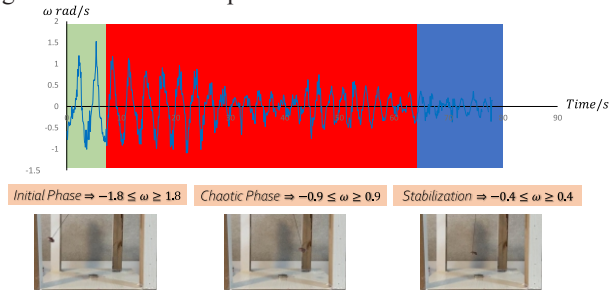


Fig. 11: Different phases

The same effect is clearly observable in the displacement-time graph, where the gradual decay of amplitude due to low damping is evident (Fig. 12).

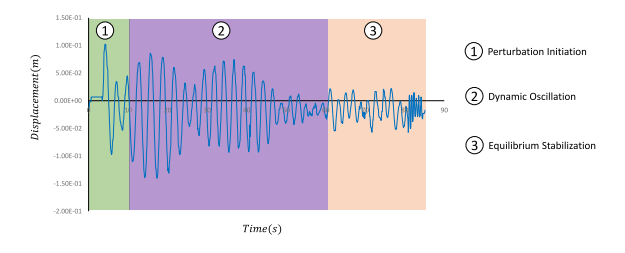


Fig. 12: Displacement

We measured the oscillation period over a defined time interval. However, due to the non-uniformity of the period across different phases, the simple harmonic motion equation is not applicable. Consequently, a modified equation was formulated to account for the time-dependent variation of the period, influenced by the pendulum's dynamics and the magnetic field (Fig. 13).

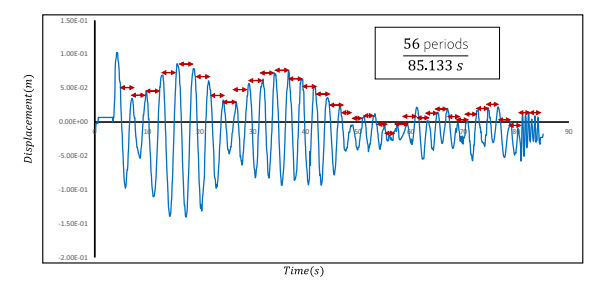
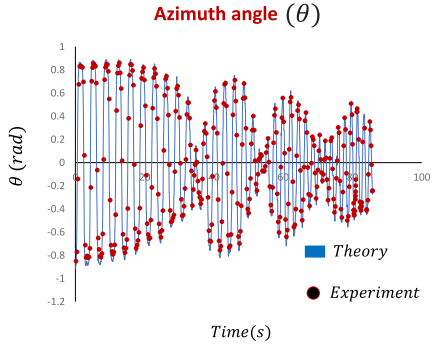


Fig. 13: Displacement vs time

Alternating period:

$$T = 4 \int_0^{\theta_{max}} \frac{d\theta}{\sqrt{\frac{2g}{l} \left(\cos(\theta) - \cos(\theta_{max}) + \frac{2\mathbf{m}B}{Ml^2} \left[\cos(\theta - \theta_B) - \cos(\theta_{max} - \theta_B)\right]}}$$

To compare pendulum angle in experiment and theory two angles, azimuth and zenith, are plotted versus time (Fig. 14).



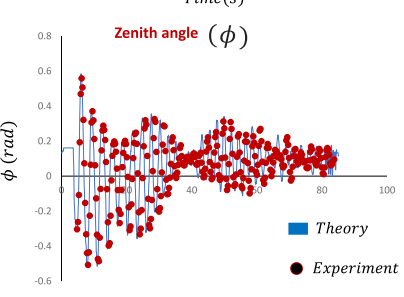
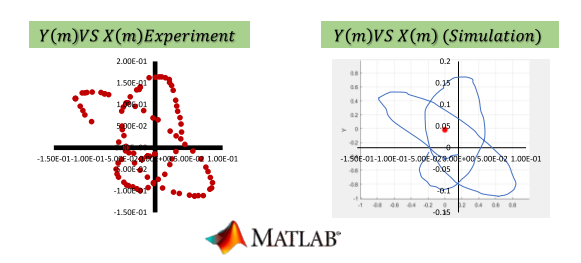


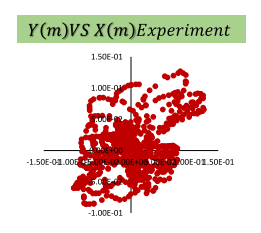
Fig. 14: Comparing azimuth and zenith angles by experiment vs theory

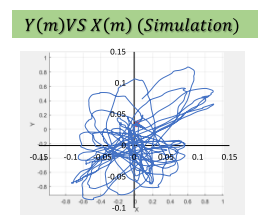
Time(s)

#### Perturbation Initiation

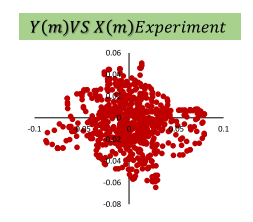


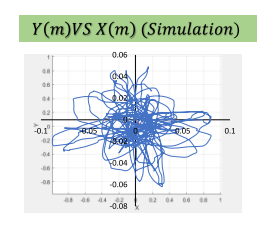
#### Dynamic Oscillation





Equilibrium Stabilization





This phenomenon involves the superposition of gravitational and magnetic potential wells. A three-dimensional plot of the combined potential illustrates that gravity forms an upward parabolic profile, whereas the magnetic field introduces a downward parabolic potential centered around the magnet's position (Fig. 15).

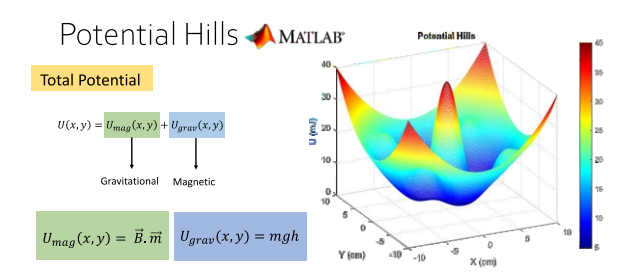


Fig. 15: Potential Hills

When the distance of the magnet increases, the magnetic potential decreases, and the gravitational potential increases. However, when the distance exceeds 8 cm, the magnetic field becomes weak, and the potential becomes 3rd Order (Fig. 16).

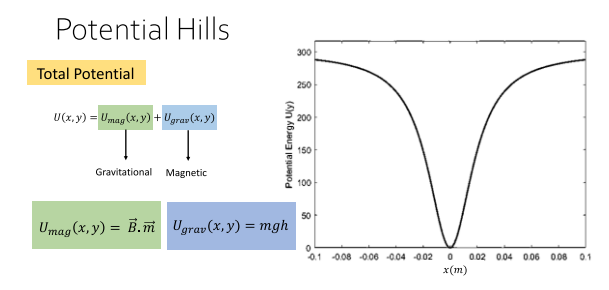


Fig. 16: Potential Hills , 3rd order

#### 4. Parameters Analysis

There are different parameters in this phenomenon which should be considered.

# A. Number of Magnets

By increasing the number of magnets, the system reaches a damped state faster and has more damping. However, the pendulum only settles within the magnetic field radius of one of the magnets to reach a stable state, which is why the graph appears this way (Fig. 17).

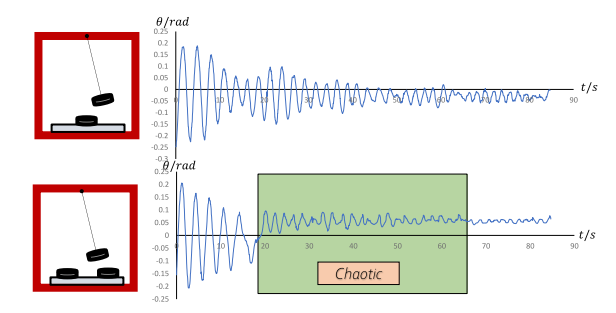


Fig. 17: The effect of number of magnets

#### B. Distance of the Magnets

In the plot of maximum angular velocity versus distance from the magnet, chaotic motion is observed up to a distance of 3 cm. Beyond this point, the motion becomes non-chaotic. The chaotic behavior is caused by the interference of the magnetic fields of the two magnets, which was confirmed in the experiment using a magnetic field mapping sheet (Fig. 18).

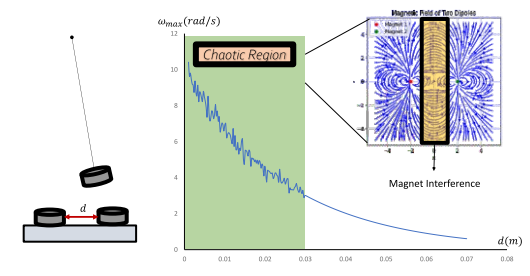


Fig. 18: Distance of the magnets

#### C. Initial Dropping

According to the theory, the motion follows a logarithmic behavior, which was also observed experimentally. When the data were fitted together, a good agreement between the theoretical prediction and the experimental results was obtained (Fig. 19).

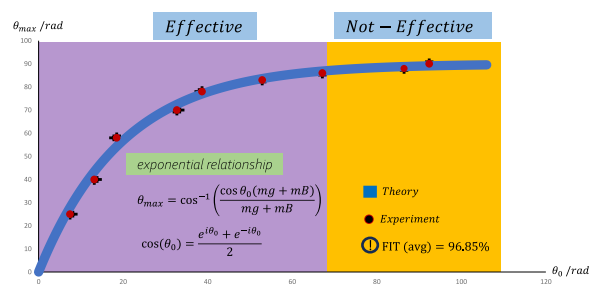
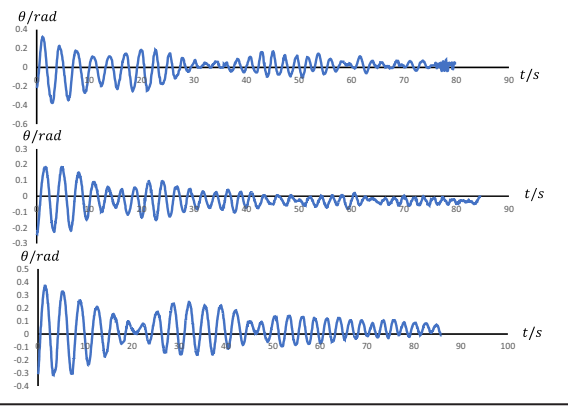


Fig. 19: Initial dropping

#### D. Distance Between 2 Magnets Down & Top





In this section, the first 10 seconds of the graph were plotted, and the amplitudes were compared. The theoretical motion equation was fitted to the experimental data, resulting in a good fit (Fig. 20).

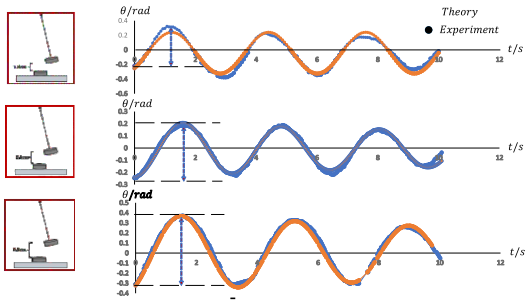


Fig. 20: Angle vs time in different positions of magnets

Frequency is inversely related to the period. Therefore, to plot the theoretical curve, the inverse of the period equation was used (Fig. 21).

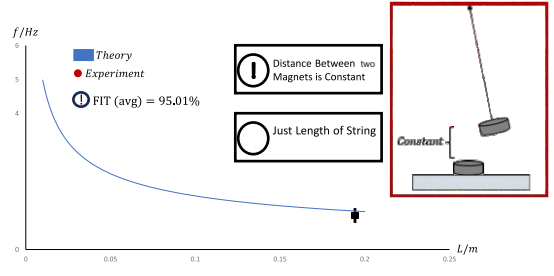


Fig. 21: Frequency Vs the Length of the String

$$f(l) = \left[4 \int_{0}^{\theta_{max}} \frac{d\theta}{\sqrt{\frac{2g}{l}(\cos(\theta) - \cos(\theta_{max}) + \frac{2\mathbf{m}B}{Ml^2}[\cos(\theta - \theta_B) - \cos(\theta_{max} - \theta_B)]}}\right]$$

# 5. Conclusion

- The magnetic field was derived in threedimensional spherical coordinates
- By the Lorentz force the magnetic force and the term for the matrix of the interaction of magnets were calculated.
- Equation of motion was derived
- Six main parameters were checked and controlled
- Magnetic filed was measured by Hall Effect Sensor
  - Damping and drag coefficient were measure
  - Based on the fit between theory and experiment, it can be concluded that in the first setup, the equations used exhibit high numerical accuracy, and the tests performed involve a well-designed setup with minimal error.

# References

 Strogatz, S. H. Nonlinear Dynamics and Chaos: With Applications to Physics, Biology, Chemistry, and Engineering. Westview Press, 2015.

- Moon, F. C., & Holmes, P. J. (1979). A magnetoelastic strange attractor. Journal of Sound and Vibration, 65(2), 275–296
- [3] Motter, A. E., Gruiz, M., Károlyi, G., & Tél, T. (2003). Doubly Transient Chaos: Generic Form of Chaos in Autonomous Dissipative Systems. Physical Review Letters, 111, 194101.

[2]

[4] Moon, F. C., & Holmes, P. J. (1979). A magnetoelastic strange attractor. Journal of Sound and Vibration, 65(2), 275–296.

# CONSTRUCTION OF A FOUR-GEL VERTICAL ELECTROPHORESIS MACHINE WITH AN ICE COOLING SYSTEM

Mahsa Hemat, Kimia Faraji

ABSTRACT

ARTICLE INFO

Accepted by Ariaian Young Innovative

Minds Institute, AYIMI

http://www.ayimi.org.info@ayimi.org

The inability to simultaneously load a large number of samples, the inability to increase the source voltage to increase the speed of the experiment, the lack of cooling systems, the high cost of cooling systems or their inefficiency in Iranian devices, the high cost of similar foreign devices, and the large volume of buffer consumed in them, led this research group to create a four-sided device by connecting several pieces of plexiglass and sealing it with chloroform

Keywords: Vertical Electrophoresis Device, Ice Cooling System, Gelation Plates, Buffer

#### 1. Introduction

A vertical electrophoresis system is a device used to separate nucleic acids and proteins. Charged particles are moved and separated by an applied electric field.

For electrophoresis, a sample containing a variety of proteins or DNA or RNA, a small amount of it, is loaded onto wells embedded in a porous network (such as acrylamide-based gels). This device has two buffer chambers and a gelation chamber, where the gel is connected to one buffer chamber at the top and to another buffer chamber at the bottom. After an electric field is established between the two buffers by applying a potential difference on both sides of this network, the molecules in the sample begin to move at different speeds within the porous network, which depend on their electric charge, molecular mass, and sometimes spatial shape, and are separated from each other. These samples appear as distinct bands after staining and are analyzed.

Different samples are loaded into the wells created by the comb in the gel. The number of wells can be varied depending on the comb teeth, but it is understandable that there is a limit to how many can be loaded into each comb. For this reason, to load a large number of samples, either the device needs to be used repeatedly, which is timeconsuming, or the gel needs to be extended. Today, various designs of devices have solved the above problem to some extent, but each has its own disadvantages. Some devices have tried to improve the problem by increasing the length of the gelation station, which has two disadvantages. First, if a small number of samples need to be loaded, a small amount of gel and buffer solution cannot be used, and the entire gelation station and buffer chambers must be filled, which is associated with material waste. Second, guiding a long comb is somewhat more difficult than guiding a short comb, and sometimes causes bubbles in the gel and wells. These disadvantages led the manufacturers of this device to add a smaller number of gelation plates to give the experimenter the power of choice so that he can choose between one or several plates for gelation, depending on the number of samples. In some countries, two-chamber, four-chamber, and even twelve-chamber devices have been designed for gelation, the most famous of which is from the Biord company. In the two-chamber samples.

House and four houses To optimize the conditions,

including controlling the increase in temperature during the experiment, the system is designed in such a way that it is immersed in a large volume of buffer. In the twelvehouse device, in addition to placing the gelation position in the buffer tank, a cooling system is also connected to the device to control the heat generated by the operation of the twelve gels containing the sample. This increase in temperature in different parts of the device and gels is the result of the increased resistance that the electrodes, the buffer used, and the gel show to the electric current, which, if not controlled, can cause undesirable results such as breaking the glass containing the gel, creating irregularities in the size of the gel pores, and damage to the device. On the other hand, when the temperature is not uniform in all parts of the gel, the shape of the separated bands is irregular and, in the so-called bands, they become smiling because the samples in the middle bands will move faster than the side rows.

In Iran, one-way and two-way devices are available on the market, in which the gel is connected to a limited buffer chamber from the top and to another limited buffer chamber from the bottom, which results in less buffer use than similar foreign models mentioned, although it should be noted that in most of them, high voltages cannot be used like similar foreign models because the temperature increases and the consequences mentioned above will follow. As a result, either the voltage must be kept at a moderate level, which slows down the speed of the test, or different cooling systems must be used, such as water circulation systems in the walls of the device or other electrical systems, which in addition to wasting electricity and water imposes a high cost on the device. The aim of this study is to load a larger volume of samples in less time using a four-way device that also saves on buffer consumption compared to similar foreign models. Each side of the device is connected to a separate chamber from above and below, which allows the experimenter to avoid filling the corresponding chambers when each side of the device is not used and to avoid unnecessary consumption of buffer. On the other hand, to prevent the use of excess electricity and sometimes water for cooling devices at high voltages, a new and cost-effective method (from an environmental and economic point of view) will be used, namely placing ice packs in the chamber created between the four plates.

#### 2. Materials and Methods

After designing the desired device, plexiglass plates were cut to appropriate sizes with a laser. After mounting the plates on each other and temporarily connecting them with paper glue, the wires and plugs were connected. The plates were connected to each other with chloroform and sealed. The empty space between each corner was filled with aquarium glue. A U-shaped line was created on each side with silicone filament to prevent the upper tank buffer from falling. The special glass for gelation was cut and attached to the device with the screws provided. A rectangular metal cube was made to fit the chamber enclosed by the device and before welding the last side, the cube was filled with gelice. After the tests were carried out to ensure the tightness of the chambers, the device was sent to Pasteur for testing and comparison with similar Iranian samples.



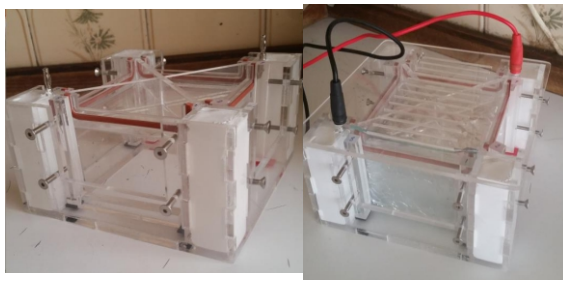


Fig. 1: The Final setup

#### 3. Results

Reducing the width of the bottom of the designed tanks and increasing the height of the walls and the cross wall at the top of the system made it possible to save on buffer consumption. The sealing of each side and the absence of leakage and the absence of buffer diffusion above when installing the glasses were confirmed by pouring water. The cooling power of the gel ice was proven by placing it in the desired chamber and examining the temperature passing through the plexiglass plate. The results of comparing the device with similar cases are being reviewed.

### 4. Conclusion

In discussions and interviews with relevant individuals, we found that although many Iranian companies manufacture and market various types of vertical electrophoresis devices, many laboratories in the country still purchase similar foreign devices due to their greater efficiency, which incurs a lot of costs and seriously damages domestic production. On the other hand, the necessary studies showed that the manufacture of these devices and their optimization do not require complex technology, and even by designing and manufacturing

more efficient models, the country can enter the global competitive market in this product and prepare the ground for its export to other countries.

Inability to simultaneously load a large number of samples, inability to increase the source voltage in order to increase the speed of the test; Without cooling systems, the high cost of cooling systems or their inefficiency in Iranian systems and the high cost of similar foreign devices and the large volume of buffer consumed in them led to the creation of a device that can mount one to four gelcontaining plates so that the detection of a large number of samples is not time-consuming and the small number does not waste materials in large systems. Although the number of samples that can be loaded in each gel depends on the number of comb teeth used, if each side normally has 10 wells, this system can load 40 samples. This device has separate and small buffer chambers for each gel, which allows for saving on buffer consumption. The ice cooling system built into the middle of the device, in addition to eliminating expensive cooling systems with high water or electricity consumption, also made it possible to increase the voltage to increase the speed of the experiment. By using this system, in addition to maintaining quality, it is possible to help conserve limited energy resources, and it is also possible to prevent the outflow of national capital by localizing the device and reducing the import of similar devices from foreign countries.

#### References

- [1] Martin, E, hine, R, dictionary of biology, new York: oxford university press, 2008.
- [2] Westerneier,R, electrophoresis in practice, Germany: Wiley-VCH, 2005.
- [3] Fox, G. F, Sep 2005 (on-line)
- [4] (http://www.google.com/patents/US6942775)
- [5] Hoffman, D, An Atlas of Protein Electrophoresis, Carolina: Department of Pathology and Laboratory Medicine, 2006.
- [6] Janson, J. C, Protein Purification, John Wiley & Sons,
- [7] Perez, E, Compact cell clamp for slab gel plate assembly, Aug 2002 {on-line}, (http://www.google.com/patents/US6436262)
- [8] Raymond, S, Vertical gel electrophoresis apparatus, Mar 1968 {on-line}, (http://www.google.com/patents/US3374166)
- [9] Perez, E, Fernwood, G, Rapid assembly casting system for slab gels, Dec 2000 {on-line} (http://www.google.com/patents/US6162342

# INVESTIGATION OF A FLUID IN A HIGH VOLTAGE

Shiva Azizpour

# ARTICLE INFO

Iran Team Member, Gold Medalist in IYPT 2012, Germany Accepted by Ariaian Young Innovative

Minds Institute, AYIMI

http://www.ayimi.org,info@ayimi.org

#### ABSTRACT

f a high voltage is applied to a fluid (e.g. deionized water) in two beakers, which are in contact, a fluid bridge may be formed. Bridge Formation, an unstable position, variation by increasing the temperature, flow visualization and sparks are initial observations. By theory the formation of such a bridge and sparks, and the stability of electrical force, surface tension and gravitation are studied. Critical voltage and reactions in the bridge should be considered too. By experiment and image processing different parameters such as deflection and voltage reduction are studied.

Keywords: Fluid, Deionized water, Beakers, Voltage

#### 1. Introduction

With connection a high voltage to a fluid (e.g. deionized water) in two beakers, a fluid bridge may be formed. Bridge Formation and sparks are initial observations which by theory and experiment different parameters in this phenomenon are studied.

This research is started by connecting two container filled with deionized water to a high voltage. The sparks will appear as the bridge breaks down. (Fig. 1).

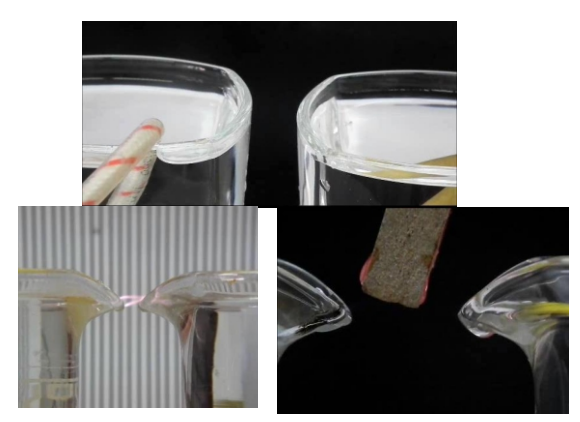


Fig. 1: Fluid bridge

But is the Bridge Always Stable? Using small colored powders we monitored the flow in two beakers to detect the water flow (Fig. 2).



Fig. 2: Using colored powder

One of the parameters which is studied in this phenomenon is temperature. An increase in the temperature of the water passing through the bridge would change the refractive index.

# 2. Theory

Force application and dipole in an electric field (Fig. 3):

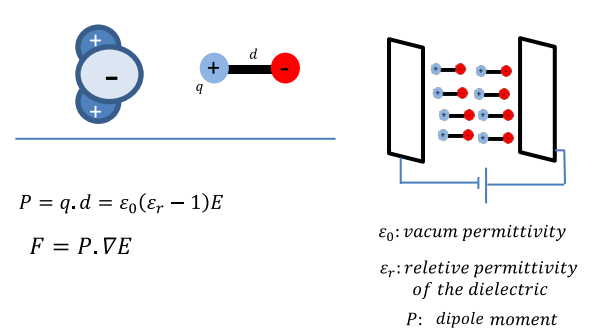
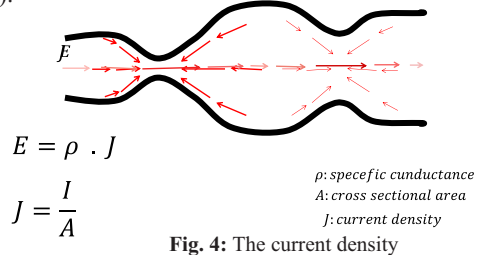


Fig. 3: Applied force

In an electric force with specific conductance and cross sectional area the current density is given as follows (Fig. 4).



But the spark is formed when the electric field strength exceeds the dielectric field strength of air (Fig. 5).

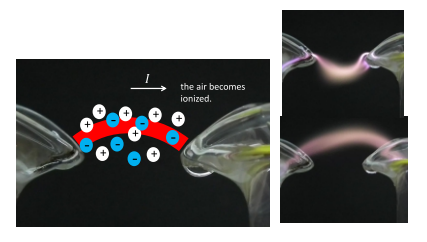


Fig. 5: the formation of sparks

The force applied to the dipoles is in the direction of

electric field's gradient (Fig. 6).

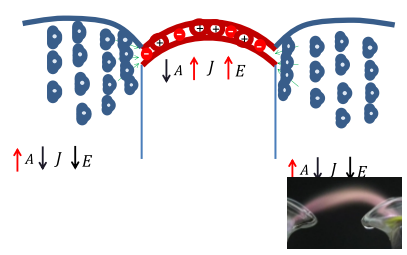


Fig. 6: Electric field's gradient

Water is a stronger conductor than air which results in a current through water rather than air. Molecules in A and C will be attracted toward B to reach a stable position (Fig. 7).

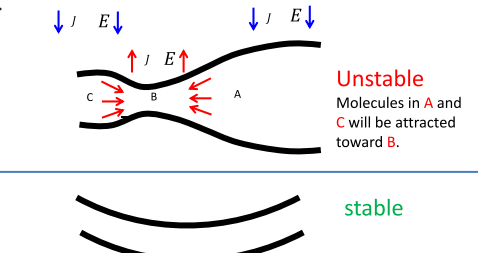


Fig. 7: Tending to the stable condition

The force applied to the volume element is in the direction of electric fields gradient.

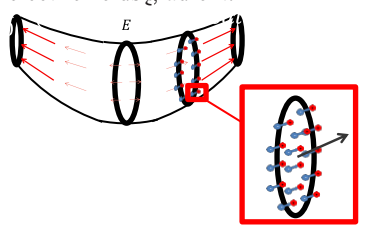
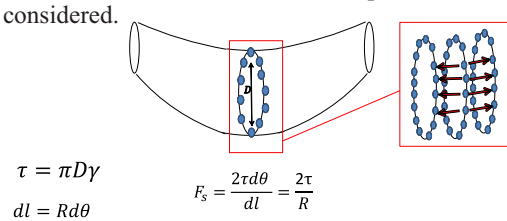


Fig. 7: Electric Force

The force applied to the surface element because of surface tension which is the other parameter should be considered.



 $\gamma : srface\ tension\ coefficient$ 

R: radius of curveture

Fig. 8: Surface Tension

Force applied to the surface element due to gravitation is other parameter but what is holding the bridge against gravity (Fig. 9)?

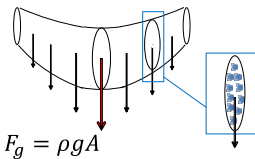


Fig 9: Gravitational force

Since there is a slight sag in the bridge the main force cancelling the gravitational force is surface tension force. The bridge is stable so in equilibrium:

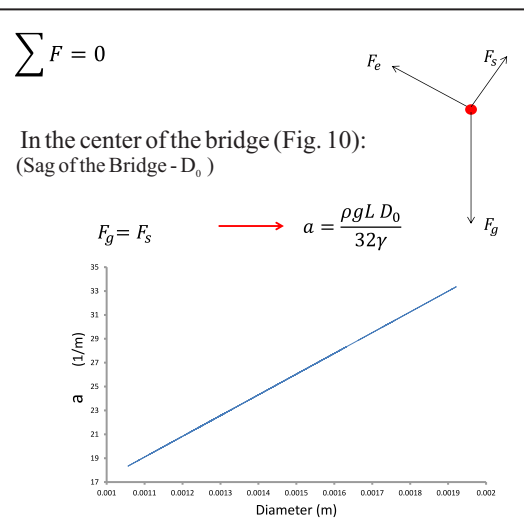
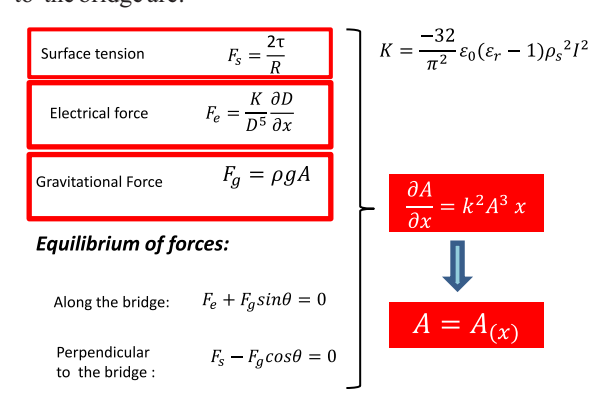


Fig. 10: a versus diameter

Equilibrium of forces along the bridge and perpendicular to the bridge are:



How to reach a limitation for stability?

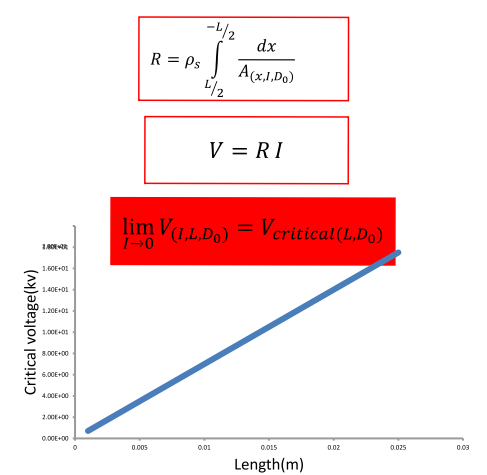


Fig. 11: Critical Voltage vs. length

#### 3. Experiments

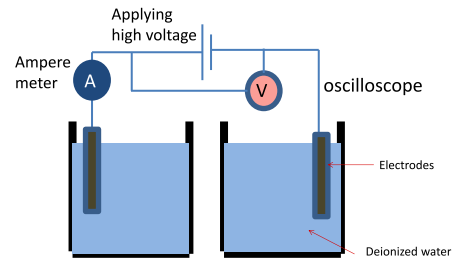
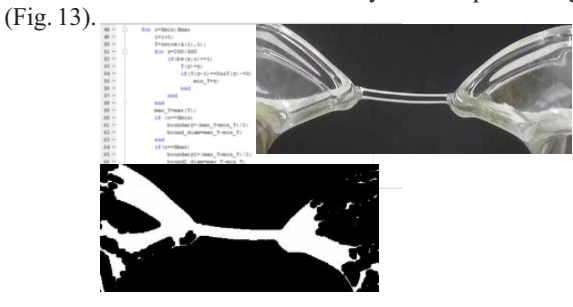




Fig. 12: Experimental setup

Diameter's oscillation is found by video processing



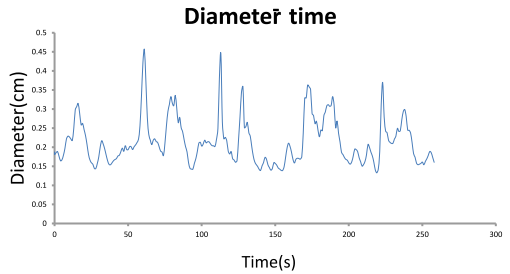
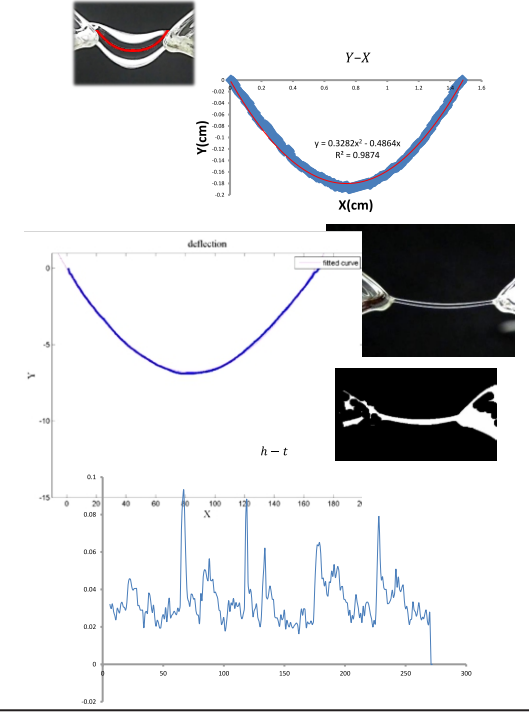


Fig. 13: Diameter vs. time

Bridge coordinate and deflection oscillation:



# 4. Statistical Operation

The diagrams of a vs. maximum diameter and changes of diameter verus X are plotted (Figs. 14 and 15).

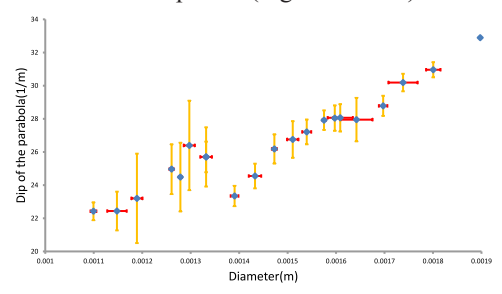


Fig. 14: a vs. maximum diameter

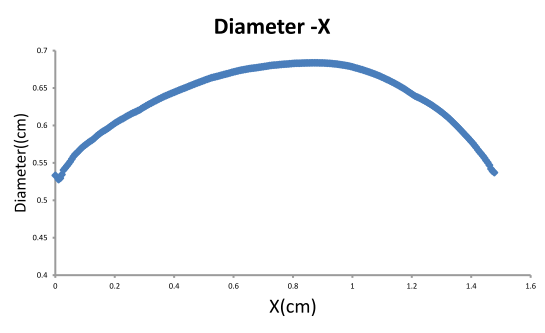


Fig. 15: Diameter vs X

The bridge is formed in different high voltages (Fig. 16) and the length and diameter of the bridge are plotted in different voltages (Figs. 17 and 18).

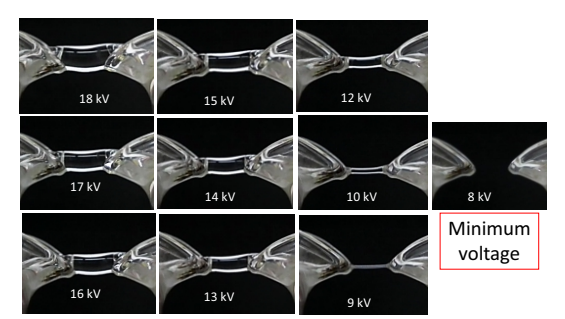


Fig. 16: Different voltages

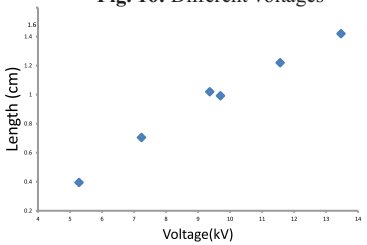


Fig. 17: Length vs voltage

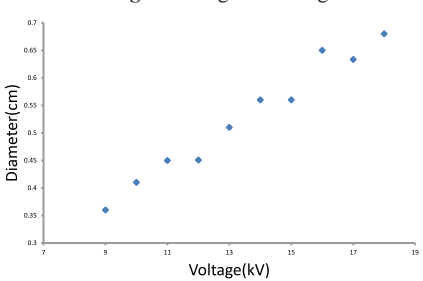
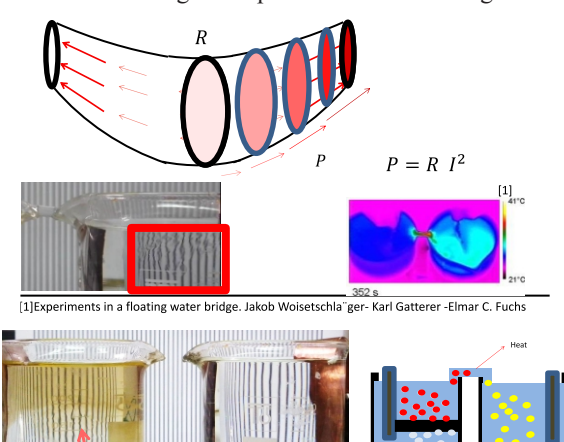


Fig. 18:Diameter vs voltage

The role of heating in this phenomenon is investigated.



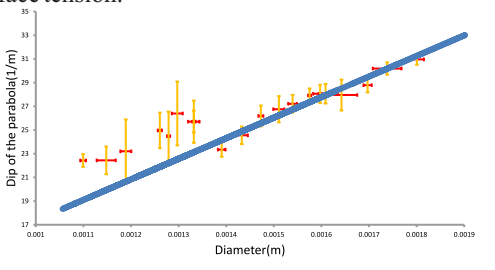
# 5. Conclusion

# Theory vs. Experiment

Stratification

What is holding the bridge?

The comparison verifies our theory which stated: The force that is holding the bridge against gravity is the surface tension.



[1] Description of Spherical Aberration and Coma of a Microlens Using Vector Diffraction Theory Glen D. Gillena and Shekhar Guhab

Length vs. minimum voltage  $\,$  and diameter vs. X shows good agreement between theory and experiment (Figs . 19

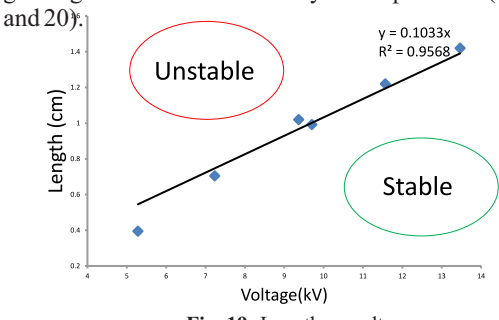


Fig. 19: Length vs voltage

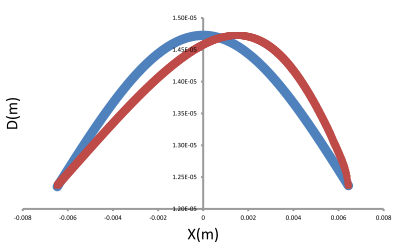


Fig. 20: Diameter vs X

# Formation

Sparks are the reason of formation and also cause the droplet ejection.

# **Stability**

The surface tension is the reason of the bridge stability.

# References

- [1] Experiments in a floating water bridge .Jakob Woisetschla" ger Æ Karl Gatterer Æ Elmar C. Fuchs(2010)
- [2] PHYSICAL REVIEW E 80, 016301 2009 Theory of the Maxwell pressure tensor and the tension in a water bridge. A. Widom, J. Swain, and J. Silverberg
- [3] Journal of Electrostatics, 26 (1991) 143-156 Elsevier. Journal of Electrostatics, 26 (1991) 143-156 Elsevier. A. Ramos and A. Castellanos

# **ROTATING RING**

Yas Meshkin et. all, Azad University

#### ABSTRACT

ARTICLE INFO

Pre registered in IPT 2025 Poland

Accepted by Ariaian Young Innovative

Minds Institute . AYIMI

http://www.ayimi.org,info@ayimi.org

Problem states when a magnetic ring is left at the top of a ferromagnetic rod, several types of motion can be observed. Under which conditions does each type of motion appear? Which types of motion lead to the longest fall time for a given ring radius?

Key Words: Magnetic Ring, Ferromagnetic Rod, Motion, Rotating

# 1. Introduction

The interaction between a magnetic ring and a ferromagnetic rod provides an intriguing demonstration of physical principles. When a magnetic ring is placed at the top of a ferromagnetic rod, its subsequent motion is governed by a combination of magnetic forces, gravitational forces, and frictional interactions at the interface between the ring and the rod. This problem allows us to explore the dynamic interplay of forces under varying conditions, leading to a spectrum of possible behaviors, including stationary states, pure rolling motion, sliding motion, and combinations of rolling and sliding.

The behavior of the system depends on several factors, such as the magnetic field strength of the ring, the material properties of the rod (e.g., its ferromagnetic nature and surface characteristics), the ring's mass and radius, and the initial conditions (e.g., whether the ring is released from rest or given an initial velocity). Additionally, external parameters such as the coefficient of friction and the presence of any external fields (e.g., gravitational or external magnetic fields) also influence the observed motion. This analysis seeks to identify and categorize the conditions under which each type of motion appears, while also determining the types of motion that maximize the fall time of the ring for a given radius. The study is framed within the context of classical mechanics and electromagnetic theory, and the findings are supported by mathematical modeling and physical reasoning.

#### 2. Physical Phenomena

- 1. Magnetic Force: The magnetic ring exerts a magnetic field that interacts with the ferromagnetic rod. This interaction produces an attractive force that influences the ring's motion. The strength and distribution of this force depend on the magnetic properties of the ring and the rod, as well as their relative positions.
- 2. Gravitational Force: The weight of the ring (, where is the mass of the ring and is the acceleration due to gravity) acts vertically downward, providing a constant driving force that influences the motion.
- 3. Frictional Force: Friction arises at the contact surface between the ring and the rod. The magnitude and the direction of this force depend on the nature of the motion (rolling, sliding, or a combination of both) and the

friction's coefficient.

- 4. Rolling Without Slipping Condition: For rolling motion to occur without slipping, the velocity of the contact point between the ring and the rod must be zero. This imposes a relationship between the translational and rotational velocities of the ring.
- 5. Energy Dissipation: Energy losses due to friction or eddy currents (induced by relative motion between the magnetic ring and the ferromagnetic rod) can significantly influence the motion. These dissipative effects must be considered to accurately describe the dynamics.

# 3. Types of Motion

- 1. Stationary State: The ring remains stationary at the top of the rod if the magnetic and frictional forces are sufficient to counteract the gravitational force. This occurs when the magnetic attraction is strong, and the coefficient of static friction is high.
- 2. Sliding Motion: If the gravitational force exceeds the maximum static friction force, the ring begins to slide down the rod. In this case, the ring does not rotate significantly, and the motion is dominated by translational movement.
- 3. Rolling Motion Without Slipping: The frictional force must provide sufficient torque to ensure that the ring rolls rather than slides. This condition is met when the rolling friction exceeds the kinetic friction.
- 4. Combination of Rolling and Sliding: When the frictional force is insufficient to maintain rolling without slipping, the ring may exhibit both rolling and sliding motion simultaneously.

# 4. Theory

Analysis of the Rotational Motion of a Ring Around a Rod We have a ring that is rotating around a rod and effectively rolling about it. In Diagram 1, as shown, the red circle represents the trajectory of the ring's center of mass. The larger circle indicates the ring's own path of motion, while the smaller circle at the center is the rod itself. Currently, there are two types of motion; fisrt, the rotational motion of the ring around its own axis and second, the circular motion of the ring around the rod. (The total motion is the sum of these two)

The first motion is translational, In this case, we treat the entire ring as a single point (its center of mass) as shown in the equation:

$$\Sigma F_x = F_B - N = rac{mV_0^2}{R-r}$$

 $\Sigma F_x$  represents the horizontal forces, which include:

- The magnetic attraction force, denoted as  $F_B$ .
- The magnetic repulsion force, denoted as N.

The net horizontal force, equals the centripetal force, which is the resultant force acting around the center. Here *V* is the speed of the center of mass, or the angular velocity of the ring around the rod (represented by the red circle in (Fig. 1).

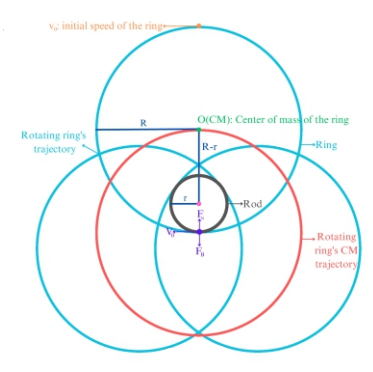


Fig. 1: Rotating ring

The second motion is the rotational motion of the ring around its own axis; The speed associated with this motion is  $V_2$  which is marked at the purple point in the diagram. At this point, the net velocity is zero, which is referred to as "rolling motion". Rolling occurs when the two speeds match.

Thus: 
$$\omega R_2 - \omega R_1 = V_0$$

Here,  $V_2$  is the initial velocity imparted to the ring, equal to Vo .

Now, let's analyze the vertical forces (shown in Fig. 2): There is a downward force, mg, due to gravity and two upward forces are present.

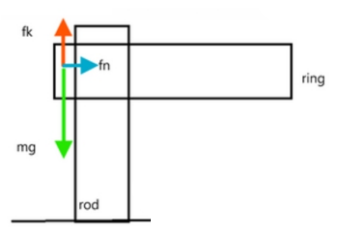


Fig. 2: The forces

$$-mg + \mu_k N + \alpha V = -m rac{dv}{dt}$$
 $-mg + \mu_k N + \alpha V - m rac{dv}{dt}$ 
 $(\mu_k N - mg) + lpha rac{dn}{dt} = -m rac{d^2n}{dt^2}$ 
 $eta + lpha rac{dn}{dt} = -m rac{d^2n}{dt^2}$ 
 $eta + lpha rac{dn}{dt} = -m rac{d^2n}{dt^2}$ 
 $eta + lpha V = -m rac{dV}{dt}$ 

$$-\frac{t}{m} = \ln\left(\frac{\beta + \alpha V}{\beta}\right)$$

$$1 + \frac{\alpha}{\beta}V = \beta e^{-\frac{t}{m}}$$

$$\alpha V = \beta e^{-\frac{t}{m}} - 1$$

$$V(t) = \frac{\beta}{\alpha} \left(e^{-\frac{t}{m}} - 1\right)$$

$$\int_0^t \frac{dt}{m} = \int_0^v \frac{dv}{\beta + \alpha V}$$

$$\frac{dn}{dt} = V \quad \Rightarrow \quad \int dn = \int_0^t \frac{\beta}{\alpha} \left(e^{-\frac{t}{m}} - 1\right) dt$$

$$-\frac{l}{\beta} \left(-\beta m e^{-\frac{t}{m}} - t\right)$$

$$\frac{\alpha l}{\beta} = s + \beta m e^{-\frac{t}{m}} + t$$

$$\beta_s = \mu_k N - mg \le \mu_k \left(F_B - \frac{mV_0^2}{R - r}\right) - mg$$

$$\beta_s = \mu_k F_B - \frac{\mu_k mV_0^2}{R - r} - \mu_k mg$$

$$i : \beta_s \rightarrow \beta e^{-\frac{t}{m}} \rightarrow 0$$

$$\frac{\alpha l}{\beta} = s + \alpha l - \beta t + 2\frac{\alpha}{\beta}l$$

$$t \rightarrow \infty$$

$$t = \frac{\alpha l}{\mu_k F_B - \mu_k mg - \frac{\mu_k mV_0^2}{R - r}}$$
The larger the value of this fraction, the longer the fall time will be.
$$V_0^2 = \frac{\mu_k mV_0^2}{R - r} - \mu_k (F_B - mg)$$

$$V_0 = \sqrt{\frac{\mu_k (F_B - mg)(R - r)}{\mu_k m}}$$

Minimum Velocity: The ring will remain stationary unless a perturbation causes it to start moving. If perturbed, the ring will begin to descend if the gravitational force exceeds the maximum static friction force, where µk is the coefficient of static friction. Maximum Velocity: As the initial velocity increases, the normal force increases due to the increased centripetal force requirement. This, in turn, increases the frictional force. If becomes sufficiently large, the upward frictional force may balance the gravitational force, reducing the net downward acceleration. As approaches a critical value, the net acceleration approaches zero, and the time required for the ring to descend becomes infinitely long. This implies that the ring would continue rotating around the rod without descending, as shown in the equations. The energy loss has been calculated as well.

# 5. Total Energy of the System

 $V_0 = \sqrt{\frac{(F_B - mg)(R - r)}{m}}$ 

The total energy consists of three main components:

# a. Kinetic Energy of Translation

The translational kinetic energy arises from the linear motion of the ring's center of mass. It is expressed as:

 $K E_{translation} = 1/2 \text{mv}^2$ , where m is the mass of the ring and V is the velocity of the ring's center of mass.

#### b. Rotational Kinetic Energy

The rotational kinetic energy arises from the ring's rotation about its own axis. It is given by:

$$KE_{
m rotation} = rac{1}{2}I\omega^2$$

where I is the moment of inertia of the ring and  $\omega$ s the angular velocity of the ring.

$$I=mR^2 \hspace{1cm} \hspace{1cm} \hspace{1cm} \hspace{1cm} \hspace{1cm} \hspace{1cm} \hspace{1cm} KE_{ ext{rotation}}=rac{1}{2}mR^2\omega^2 \hspace{1cm} \hspace{1c$$

# c. Potential Energy Due to Gravity PE = mgh

As the ring moves, energy is dissipated due to two primary mechanisms: friction and eddy currents.

# a. Frictional Dissipation

Friction between the ring and the rod leads to energy loss. This dissipation power is given by: Pfriction =  $\mu kN v$ , where  $\mu k$  is the coefficient of kinetic friction and N is the normal force(influenced by the magnetic and gravitational forces), vis the velocity of the ring's center of mass.

# b. Eddy Current Dissipation

When the ring moves in the magnetic field of the rod, eddy currents are induced within the ring. These currents produce resistive forces (in accordance with Lenz's Law) that dissipate energy. The power loss due to eddy currents is given by:

$$P_{
m eddy} = rac{dE_{
m eddy}}{dt}$$

The total dissipation power is the sum of frictional and eddy current losses:

$$P_{
m loss} = \mu_k N v + rac{dE_{
m eddy}}{dt}$$

The critical velocity serves as the threshold for determining whether rolling or sliding motion dominates. Below this velocity, frictional forces are sufficient to maintain rolling, while above it, sliding occurs as friction becomes insufficient. This velocity is influenced by the coefficient of friction and magnetic force. Additionally, the material properties of the rod, such as magnetic permeability and electrical conductivity, play a crucial role in the system's dynamics by affecting the magnetic force and eddy current damping. Stability of motion is determined by the balance of frictional, gravitational, and magnetic forces, which counteract perturbations to maintain consistent rolling or sliding. The time to fall is dependent on factors like initial velocity, friction, and magnetic force, with rolling leading to a slower descent due to controlled energy dissipation through friction and eddy currents. The system's motion is governed by the interplay of critical velocity, material properties, stability, and energy dissipation mechanisms. Rolling motion occurs when friction and magnetic forces maintain stability, while sliding dominates when these forces are insufficient. The rod's material properties influence both the magnetic force and energy loss through eddy currents, directly affecting the ring's motion. Energy dissipation reduces the system's total mechanical energy, impacting the fall time.

These theoretical insights provide a comprehensive understanding of the ring's dynamics and establish a framework for experimental validation, focusing on how varying initial conditions and system parameters influence motion.

#### 6. Conditions Leading to Maximum Fall Time

1. High Magnetic Force:

A strong magnetic attraction, enhances frictional resistance and reduces the ring's acceleration.

2. Rolling Motion Without Slipping:

Rolling motion dissipates energy slower than sliding, leading to longer fall times. The rolling condition is favored by a high coefficient of friction and sufficient torque generated by the magnetic force.

3. Eddy Current Effects:

In some cases, eddy currents induced in the ferromagnetic rod by the moving magnetic ring can create opposing forces that slow the motion, further increasing the fall time.

#### 4. Low Initial Velocity:

Reduces kinetic energy, giving the ring more time to transition into a rolling state where energy dissipation is minimal. Higher initial velocities can lead to sliding or a combination of rolling and sliding, which accelerates the fall.

# 5. High Coefficient of Friction:

This maximizes the time spent in a slow, rolling descent and ensures the ring transitions into rolling motion more easily by counteracting sliding forces.

6. Large Ring Radius:

Increases the moment of inertia, reducing angular acceleration which slows down the overall motion as more torque is required to overcome the rotational inertia.

7. Optimal Rod Material Properties:

A ferromagnetic rod with high magnetic permeability, to maximize the magnetic force ().

8. Balance of Magnetic and Gravitational Forces: Results in a quasi-stationary state where the net force is minimal.

#### Minimal Perturbations :

External disturbances, such as vibrations or additional forces, can disrupt rolling motion or stationary conditions, leading to faster descent.

10. Low Energy Dissipation Through Friction: Moderate friction levels ensure rolling without excessive energy loss due to heat dissipation, maintaining a slow but steady motion.

# 11. Symmetry and Uniformity of the Ring:

A perfectly symmetric and uniformly dense ring even distribution of forces and moments of inertia. Any asymmetry could introduce wobbling or uneven rolling, potentially accelerating the fall.

# 12. Rod Orientation:

A perfectly vertical rod ensures the gravitational force is fully aligned with the motion. Any deviation (e.g., a tilted rod) introduces a horizontal component of gravity, which may reduce friction's effectiveness and speed up the descent.

# 13. Environmental Factors:

Air Resistance: In cases where the ring moves faster (e.g., due to sliding), air resistance could add additional damping, indirectly affecting the time. However, its effect is usually negligible for small, dense objects. Temperature: Higher temperatures might alter the properties of the rod or the coefficient of friction, impacting the motion.

14. Ring Material Properties: A ring with high electrical conductivity will induce stronger eddy currents as it interacts with the ferromagnetic rod. This creates additional opposing forces, further slowing the descent. The magnetic susceptibility of the ring material also impacts how strongly it interacts with the rod's magnetic field.

with the rod's magnetic field.

#### 15. Surface Finish of the Rod:

A smoother rod surface reduces mechanical friction and may increase sliding motion, while a rougher surface increases friction and promotes rolling, potentially lengthening the fall time.

#### 16. Rotational Frequency Matching:

If the ring's natural rotational frequency matches the oscillatory effects (e.g., due to vibrations in the rod), it could lead to resonance effects that affect the motion. This could either stabilize or destabilize rolling motion, depending on the conditions.

#### 17. Absence of External Vibrations:

External vibrations or oscillations in the rod or surrounding environment could destabilize the ring's rolling motion, leading to increased sliding and a faster descent.

#### 18. Size of the Rod:

A thinner rod relative to the ring's size creates a smaller rolling radius, which increases the rolling resistance and can lead to a slower descent.

#### 7. Experiment

To experimentally validate the theoretical framework outlined above, we designed an experimental setup as follows: A vertical ferromagnetic rod was secured to a rigid base to ensure stability. The rod's surface was polished to control the coefficient of friction, Magnetic rings of various radius and mass distributions were prepared. Eddy current effects were evaluated using rods made of different materials (e.g., aluminum, steel, and non-magnetic alloys).

#### 7.1. Procedure

Each ring was placed at the top of the rod under controlled conditions, using a launcher capable of precise adjustments. The motion of the ring (rolling, sliding, or combined motion) was recorded at high resolution to observe transitions between different motion types. Repeated trials were conducted for each ring and rod combination to ensure reliability.

#### 7.2. Observations

Rings with strong magnetic forces exhibited prolonged descent times, indicating that increased normal forces enhanced rolling resistance. At higher initial velocities, rings transitioned from rolling to combined motion, with faster descent rates.

Eddy currents in conductive rod materials (e.g., aluminum) created significant drag forces, effectively increasing descent times by up to 30% compared to nonconductive rods. In rods with low friction coefficients, sliding dominated, leading to shorter fall times.

#### 8. Results

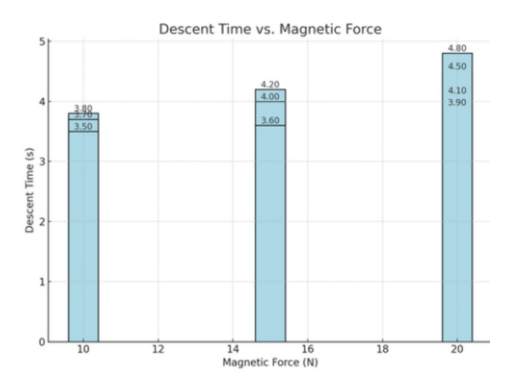
The longest descent times occurred under high magnetic attraction, low initial velocity, and non-conductive rod materials. Experimentally determined critical velocities closely matched theoretical predictions, with deviations within 5%. Transition points between rolling and combined motion aligned with theoretical frictional limits, validating the model. Eddy currents in conductive rods significantly impacted descent times, highlighting energy dissipation effects. These results confirm the strong alignment between theory and experiment, underscoring the model's robustness in describing the system's dynamics.

#### 8.1. Comparison of Theory and Experiment

The experimental findings consistently supported the theoretical predictions. Descent times for various conditions matched theoretical calculations, with longer times for rings under higher magnetic attraction and rolling motion. Critical velocities were experimentally verified within a 5% margin, validating the derived equations. Observed transitions between rolling, sliding, and combined motion adhered to theoretical conditions, with friction coefficients and magnetic forces playing critical roles. The impact of eddy currents further confirmed the theoretical consideration of energy dissipation. Overall, the results emphasize the model's predictive power and practical applicability.

The diagrams collectively illustrate how the descent time of a ring is influenced by its radius, magnetic force, and mass (Fig. 3). In the scatter plot, descent time increases with smaller radii and higher magnetic forces, as indicated by lighter-colored markers. Larger radii and lower magnetic forces correspond to shorter descent times, showing the interplay between size, friction, and resistive effects.

Marker sizes also highlight the influence of mass, with heavier rings exhibiting slightly different dynamics due to increased inertia. The bar chart complements this by showing a clear positive correlation between magnetic force and descent time. For instance, at 10 N, the descent time is around 3. 5- 3.8 seconds, while at 20 N, it rises to 4.8 seconds. This demonstrates that higher magnetic forces enhance friction and damping effects, slowing the descent. Together, these diagrams emphasize how radius, magnetic force, and mass interact to determine the descent behavior of the ring, with magnetic force playing a significant role in prolonging motion.



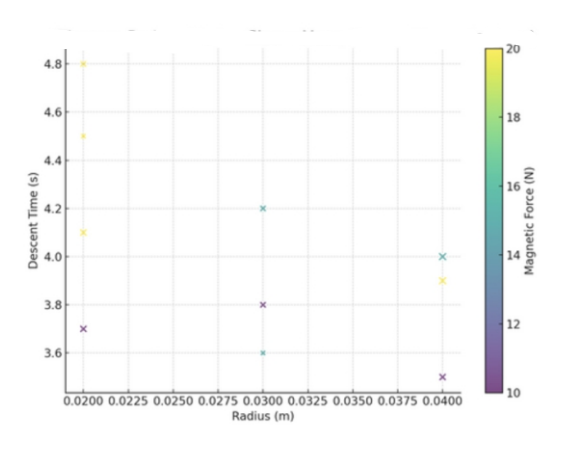


Fig. 3: Decent Time vs. Radius (Marker Size= Mass, Color = Magnetic Force

#### Experimental Data on magnetic ring's motion:

Trial	Material of Rod	Magnetic Ring Mass (g)	Initial Magnetic Field (mT)	Ring Temperature (°C)	Observed Motion Type	Fall Time (s)
- 1	Iron	50	200	25	Oscillatory	15.2
2	Iron	100	300	25	Steady Fall	8.3
3	Nickel	50	250	30	Oscillatory	16.8
4	Nickel	100	350	30	Steady Fall	7.9
5	Cobalt	50	200	25	Rotational	20.5
6	Cobalt	100	300	25	Steady Fall	8.1
7	Iron	75	275	27	Oscillatory	18.3
8	Nickel	75	275	27	Rotational	19.4
9	Cobalt	50	250	30	Steady Fall	8.0
10	Iron	100	350	25	Oscillatory	16.0

#### Experimental Data on maximum fall time:

Trial	Material of Rod	Magnetic Ring Mass (g)	Ring Temperature (°C)	Observed Motion Type	Fall Time (s)
1	Cobalt	125	25.1	Oscillatory	31
2	Cobalt	125	18.9	Oscillatory	31
3	Cobalt	125	19.0	Oscillatory	32
4	Cobalt	125	22.1	Oscillatory	32
5	Cobalt	125	21.4	Oscillatory	33
6	Cobalt	125	23.7	Oscillatory	31
7	Cobalt	125	21.2	Oscillatory	29
8	Cobalt	125	19.3	Oscillatory	30
9	Cobalt	125	21.2	Oscillatory	32
10	Cobalt	125	22.2	Oscillatory	29

#### 9. Conclusion

This study delved into the theoretical dynamics governing the interaction of a magnetic ring with a ferromagnetic rod, focusing on the intricate balance of magnetic, frictional, and gravitational forces. The theoretical framework provided a detailed classification of possible motion types-oscillatory, rotational, and steady descent-and identified the key factors influencing each. Central to the theory were parameters such as the magnetic field strength, ring mass, radius, and the material properties of both the rod and the ring, which were shown to govern the stability and transitions between motion regimes.

The theory also explored the role of energy dissipation mechanisms, including eddy currents in conductive rods and frictional forces at the ring-rod interface. These elements were modeled to predict their impact on descent times and motion stability, offering a clear explanation for the conditions under which prolonged descent or oscillatory behavior might occur. Notably, the theoretical predictions emphasized the significance of temperaturedependent magnetic properties and non-linear frictional effects, providing a comprehensive understanding of how external conditions modulate the observed dynamics. While experimental results confirmed the robustness of the theoretical models, the emphasis of this study remained on the predictive power and versatility of the theoretical framework. This work not only advances the understanding of magnetic motion dynamics but also establishes a foundation for further theoretical investigations, particularly in exploring non-uniform magnetic fields, anisotropic materials, and complex surface interactions. The theoretical insights presented here pave the way for innovations in related fields, including precision material testing, magnetic levitation systems, and dynamic stability analysis in magnetic applications.

- [1] Halliday, D., Resnick, R., & Walker, J. Fundamentals of Physics (10th Edition).
- [2] Stewart, James. Calculus: Early Transcendentals. 8th Edition.

# WATERCOURSE BLOCKAGE DETECTION SYSTEM

Fatemeh Mazdarani, Farzanegan high School

# ARTICLEINFO

Advisor: Elahe Farmad Accepted by Ariaian Young Innovative Minds Institute, AYIMI

http://www.ayimi.org,info@ayimi.org

#### ABSTRACT

he blockage of waterways in the city due to the accumulation of garbage or other reasons causes disruption to pedestrian and vehicle traffic, as well as pollution and the accumulation of rats and vermin around these waterways. Addressing these issues in a timely manner can be effective in maintaining order and cleanliness in urban life. The main core of this system is a Raspberry Pi board that, on the one hand, acts as a controller and reads the information received from the sensor designed to detect the condition of the waterway/crossing, and on the other hand, acts as a server and provides access to the information read from the sensor via the Internet.

Keywords: Blockage, Waterways, Raspberry Pi Board, Internet

#### 1. Introduction

The waste that is thrown into the watercourses accumulates after a while and causes the watercourses to become clogged and the water flow stops and the water in the watercourse flows into the alleys and streets. In addition, the blockage of the watercourses causes animals such as rats and vermin, etc. to gather around the watercourses. These animals endanger human health.

On the other hand, the watercourses that are on large and main streets, if clogged, cause a loss of order on the streets and sometimes cause traffic accidents and lead to loss of life and property (Fig. 1).



Fig. 1: Street pollution due to clogged water channels

Preventing the clogging of watercourses prevents pollution in the city and the resulting congestion and helps the municipality to keep the city clean and orderly. And because information about watercourses and their clogging does not reach the municipal organization which is responsible for beautifying and controlling the city quickly, addressing this problem is either delayed or sometimes not addressed at all. To create a fast connection between water channels and the municipal organization (or any other site), the new concept of the Internet of Things can be used. Today, the concept of the Internet of Things is used for the fast exchange of information between objects and individuals or organizations. The Internet of Things (IOT) is a new concept in the world of technology and communications, and in short, the Internet of Things is a modern technology that provides any creature (human, animal, and object) with the ability to send data via the Internet. One of the simplest and most understandable examples of the applications of the

Internet of Things is a thermostat that is installed in your home and you can control the temperature of your home wherever you are with your mobile phone. The concept of the Internet of Things led to the idea of building a device that can establish a good connection between the system that will be installed inside the water channels and the destination server. As a result, it is possible to detect the blockage of the water channels and quickly transfer this information to the municipal organization. In the rest of this article, we will explain this idea in full.

### 2. Research Background and Scientific Laws

Given that the topic of Internet of Things has only recently been used in research, projects related to this topic are very few.

Preparations for creating a smart city in cooperation with the University of Science and Technology, and in addition, the National Gas Company is working to exploit this technology in the field of gas transmission. Currently the smart city is one of the parts of this system that allows the city lights to be turned on and off and traffic control to be controlled intelligently. Another part of this system is (Ehealth), through which the patient is in contact with his doctor to receive medical advice in times of need.

# 3. Complete Definition and Description of the Components of the Project and Devices Used 3.1. Raspberry Pi Board:

One of the most important devices used in this project is the Raspberry Pi board. This board is a very small and inexpensive computer with all the capabilities of a real computer that can be used in robotics, automation, Internet of Things systems, etc. This board has pins for digital input and has the ability to connect to the Internet (Fig. 2).



Fig. 2: A view of a Raspberry Pi 1 board.

The schematic of the pins of the Raspberry Pi 2 board is shown here (Fig. 3).

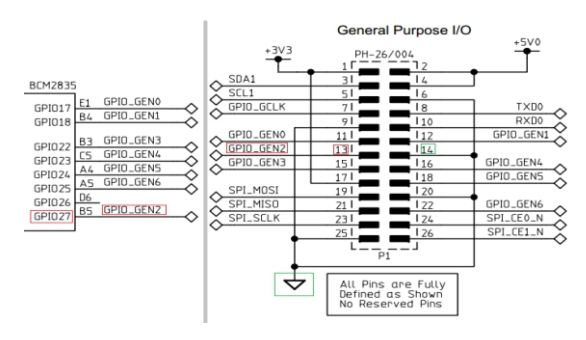


Fig. 3: Raspberry Pi 2 pin schematic

Each of the pins on the board is dedicated to a specific task. A number of these pins can be used to read digital input.

#### 3.2. Sensor

The sensor of this system consists of a floating ball and a floating rod. When the water channel is clogged and the water level rises, the floating ball and rod also rise, and finally, when the rod becomes horizontal, an electrical circuit is closed.

Sensors are working in two states of high water level (clogged) and low water level (proper condition) (Fig. 4).



Fig. 4: Sensors in two states

#### 3.3. Server

Apache server was used for the software part of the system and to bring up the site to display the status of the streams. Web Apache server is a web server program that plays a key role in the development of the web world. In 2009, Apache was the first web server program that served about 100 million website. Apache also played a key role in the development of the early World Wide Web. This server is commonly used in Unix and Linux-based environments.

#### 3.4. Coding and Languages Used

PHP, JavaScript, and HTML programming languages were used to communicate between the board and the user, and the concept of Ajax was also used to display information in the form of online graphs on the site. Ajax (Asynchronous JavaScript And XML) is a set of web standards and technologies. Using these technologies and with the help of transferring small pieces of data and information from the server, web pages react appropriately to events and it is no longer necessary to reload the web page to do anything. Notifications related to Gmail and social networks such as Telegram or Facebook, and other familiar names, are examples of the use of Ajax.

#### 4. Materials and Methods

The operating method and working method of this system consists of three parts: server, sensor, and controller (processor). The relationship between these components and the environment is as follows.

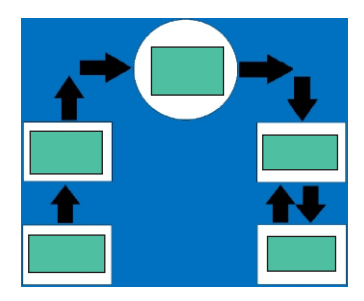


Fig. 6: System components and environment

#### Part One: Sensor

As mentioned, the device sensor consists of a ball and a floating rod, which can be detected by checking whether the electrical circuit between the floating rod and the Raspberry Pi board is closed or not.

One of the positive points of this sensor structure is its low cost, and in addition, because each board has many pins, by connecting each of the sensors to these pins, a large number of sensors and water channels can be controlled with each board.

And finally, to test the system's performance, we used a circuit as a sensor simulator and by manually connecting and disconnecting the circuit, we simulated the clogged state of the water channel and the correct state of the channel.

#### Part Two: Controller

At any moment, a request is sent from the server to check the status of the electrical circuit to learn about the status of a water channel.

The Raspberry Pi board, as a processor, reads the status of the pins connected to the sensor (if the electrical circuit is closed, the status of the pins is different from the state when the electrical circuit is not closed) and finally provides the status of the pins to the server in the form of zero and one data. This connection between the server and the processor and the Raspberry Pi board is made using the concept of the Internet of Things.

#### Part Three: Server and Site

Finally we designed a site to display information to the user and launched it on the local network using the Apache web server and in the early stages of development. 14 We used an online graph to display information related to each body of water. This graph is based on time and the state of the water, which you can see in Figure 7. This type of graph uses the AJAX technique and can see the history of the weather conditions a few moments ago.

#### 5. Data analysis and Conclusion

Today, the Internet of Things is one of the newest computer concepts that has had a significant impact on the advancement of technology.

As in this project, the Internet of Things is one of the practical and necessary concepts given that the projects carried out related to the concept of the Internet of Things in Iran are very few, this project can be a step forward to expand the use of the Internet of Things in Iran.

The remarkable point of this project is its low cost. Given that the sensor used in this system is very simple and cheap, and in addition, each Raspberry Pi board has the ability to control several sensors simultaneously, the overall cost of this system is very low in a situation where it has not yet reached the production stage. However, if this project reaches the production stage, a special controller for this system can be designed, which is naturally simpler than the Raspberry Pi board, which will

again reduce the overall cost of this system.

The sensor of this system will be placed inside the water channel and the Raspberry Pi board will be placed at a point further away from the water channels to protect it from damage caused by moisture around the water channels. The next stages of the project should be to find a suitable place for the board. Given that the structure of this system is resistant to humid environments, this system can also be used in underground channels. Another application for this structure is to control the duration of irrigation of agricultural lands in the traditional way. It is hoped that this system can take a step towards making cities smarter and providing better services to citizens.

- [1] http://www.entekhab.ir/fa/news/252523/
- [2] https://jitm.ut.ac.ir/article\_55760\_0.html
- [3] https://www.raspberrypi.org/documentation/hardware/raspberrypi/schematics/README.md

# **SPRING HYSTERESIS**

Bahareh Asadi, Farzanegan 2 School, baharehasadi 345@gmail.com

#### ABSTRACT

#### ARTICLE INFO

Iran Team Member in IYPT 2025, Lund University, Sweden

Advisor: Mohammad Mahdi Shariatmadar

Accepted by Ariaian Young Innovative

Minds Institute, AYIMI

http://www.ayimi.org,info@ayimi.org

he problem asks us to create a simple system of two identical linear springs connected symmetrically to a mass in a V-shaped configuration, with an additional adjustable external force applied to the mass. As this force is varied, under certain conditions the equilibrium position of the mass demonstrates strong dependence on the history of changes in the external force, exhibiting hysteresis which we are going to investigate.

Keywords: Spring, Hysteresis, Symmetrically, External Force

#### 1. Introduction

Hysteresis is a nonlinear phenomenon, in which the behavior of a system depends on its history. This is in direct contrast to most ordinary physical systems, whose behavior can be uniquely predicted based solely on their current state. Hysteresis-related phenomena are rare in nature, and it only appears in specific fringe cases with materials that exhibit uncommon properties.

In this research we present the analytic theory of a simple mechanical system that demonstrates hysteresis. It only consists of two ordinary springs and a mass. Given that the average person has experience with springs and gravity on a daily basis, the source of hysteresis is easy to understand, and its physical significance is very clear. Mathematically, variations of the external force cause the system to undergo two saddle-node bifurcations at two differing critical points, leading separately to the creation and destruction of branches of stable equilibria.

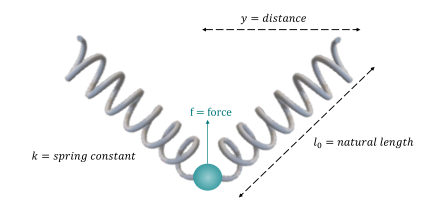
Bifurcation theory may be used to characterize a wide range of phenomena in dynamical systems .Recently, Ong has helped to address this gap in the literature by presenting an analysis of a simple mass—spring system suitable for practical demonstrations of critical transitions. In particular, he has shown that variations in an external forcing parameter can lead to saddle node bifurcations and hysteresis. Ong's treatment is well motivated and compelling, and represents a valuable addition to the literature on how critical transitions can be explored in a laboratory setting using basic equipment.

#### 2. Theoretical Model

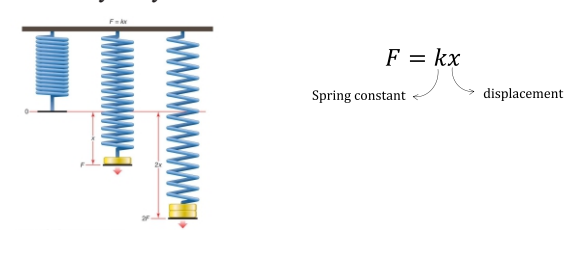
In this problem three modes of springs are studied (Fig.



Fig. 1: Three modes of spring



The springs are assumed to have linear elastic properties, so that they obey Hooke's Law.



Each spring has a characteristic stress to strain relation, governing the elastic limit of the spring. While the spring is in the elastic zone, we can use hooks law to investigate its behavior. Further deforming the spring out of its elastic zone can lead to permanent alterations in spring length and properties. Therefore, we only stretched springs in their elastic zone to prevent disfiguration (Fig. 2).

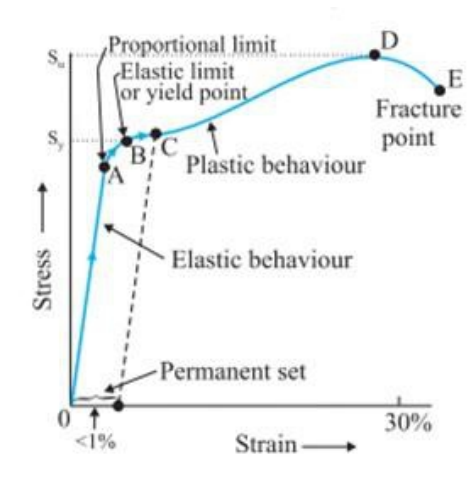


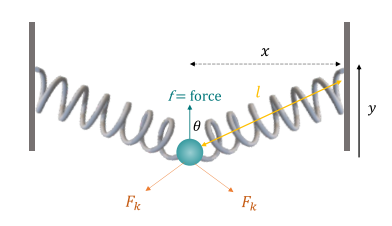
Fig. 2: Stress-Strain diagram

41

$$l(y) = \sqrt{y^2 + x^2}$$

hooke's law  $\longrightarrow$   $F_k = k (l_0 - l)$ 

$$F_k(y) = k (l_0 - \sqrt{y^2 + x^2})$$



where;

x = half the horizontal distance

 $k = spring\ constant$ 

 $l_0 = natural spring length$ 

F = net force

f = external controllable force

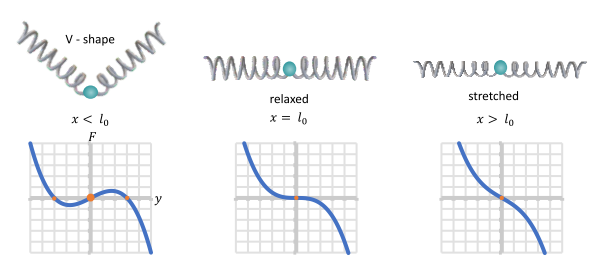
y = vertical displacement

$$F = f - 2 F_k \cos \theta$$

$$F = f - 2k(l_0 - \sqrt{y^2 + x^2}) \frac{y}{\sqrt{y^2 + x^2}}$$

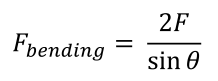
$$F = f - 2ky(1 - \frac{l_0}{\sqrt{x^2 + y^2}})$$

The system is in equilibrium when F = 0



While doing the experiments, we can observe that the springs don't always contract ideally, in contrast to our expectations, the springs bend before snapping to the second equilibrium. Here is the formula for the force required for bending one spring.

$$F = \frac{d^4 G}{32 D N_a \rho}$$





where;

F = required force for bending one spring $N_a = number of active coils$   $G = Shear\ Modulus$ 

d = Wire Diameter

D = spring diameter

 $\rho = radius \ of \ curvature$ 

Starting with a very negative value of f there is only equilibrium in the negative direction. As f becomes less negative, a new value of g appears at the critical value  $f=f_1$ . This is the onset of a saddle-node bifurcation. Further increasing g produces yet another equilibrium, or three equilibria in total. The smallest and largest g are both stable equilibrium points, whereas the central g value is unstable. Another saddle-node bifurcation occurs at the next critical value g g Here, the originally central g and the rightmost g merge together, forming a single g value. Beyond g g g the merged g vanishes, leaving behind only one g that is a stable equilibrium position (Fig. 3).

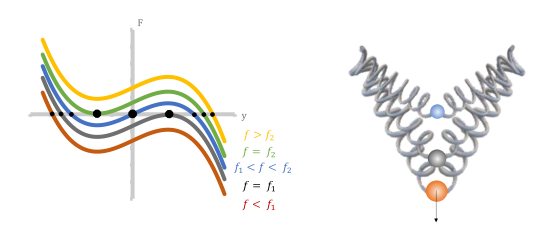


Fig. 3: External forces

Hysteresis is the dependence of the state of a system on its history. The system's output is influenced not only by the current input but also by its past inputs and the path taken to reach the current state (Fig. 4).

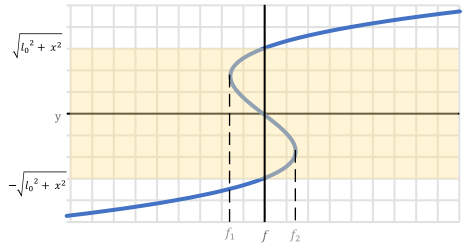


Fig. 4: Hysteresis

Imagine starting out at  $f < f_i$ , so that the state of the system initially lies on the lower stable branch. If we now increase funtil  $f_i < f < f_2$ , even though there now exist two other possible branches of y, the system will remain on the lower stable branch. This is characteristic of a stable equilibrium point, which draws the system to remain in its vicinity.

When  $f > f_2$ , the lower stable branch disappears, forcing the mass to position itself on the upper stable branch.

If we now lower f back to the region, rather than returning to the lower stable branch, the system instead tends to stay on the upper stable branch. The system only returns to the lower stable branch when  $f < f_i$ .

In this way the number of equilibria changes as the parameter space coordinates of the system (X,a) cross the critical curve. If the spring separation is held fixed with  $X < L_o$ , but f varied, then the qualitative change in the system at  $a = \pm ac$  occurs as a saddle–node. bifurcation (see Section 4). Alternatively, if the forcing is held fixed with |a| < 1, but the spring separation X varied, then the qualitative change in the system occurs as a pitchfork bifurcation (Fig. 5).

<sup>\*</sup> upwards direction is taken to be positive

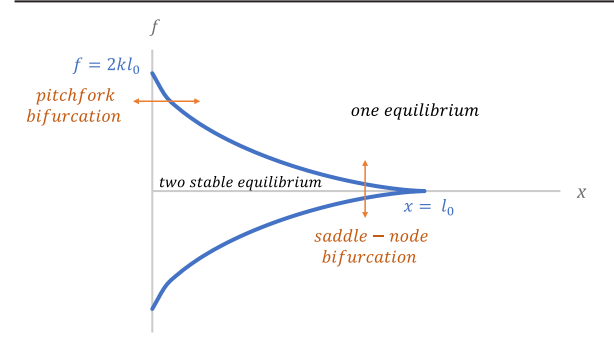


Fig. 5: Bifurcations

we study pitchfork bifurcations by exploring how the number of possible equilibria changes if the separation x is varied instead, with other factors held fixed.

In perfect pitchfork bifurcations we try to solve the above equation if external force=0. Notice that if  $x > L_0$ , then the springs are under tension, such that only one equilibrium is possible, with the mass at the center. If  $x < L_0$ , however, then three equilibria are permitted: two stable, symmetric equilibria with the springs relaxed at the natural length and one unstable equilibrium , with the springs pushing against each other (Fig. 6).

$$0 = f - 2ky(1 - \frac{l_0}{\sqrt{x^2 + y^2}})$$

If f = 0:

$$y = 0 \qquad or \qquad y = \pm \sqrt{l_0^2 - x^2}$$

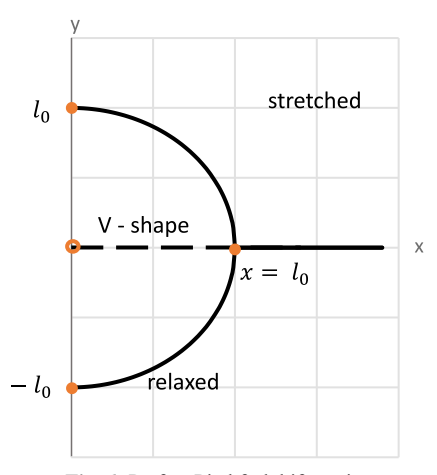


Fig. 6: Perfect Pitchfork bifurcations

If external force exceeds 0, we can demonstrate that the number of possible equilibria changes from three to one (or vice versa) whenever x passes through the critical value . In this case, the change in the number of possible equilibrium configurations is called an imperfect pitchfork bifurcation. It may be shown for the imperfect pitchfork bifurcation that increasing x e.g., by pulling the points of attachment apart from one-another can lead to the system shifting from a stable equilibrium configuration  $y < y_c < 0$  (with the mass above the springs) to the one with  $0 < y < y_s$  (mass below the springs) (Fig. 7).

$$0 = f - 2ky(1 - \frac{l_0}{\sqrt{x^2 + y^2}})$$

If  $f \neq 0$ :

$$x_c = l_0 [1 - (f/2l_0k)^{2/3}]^{3/2}$$
  
 $y_c = [l_0^{2/3} x_c^{4/3} - x_c^2]^{1/2}$ 

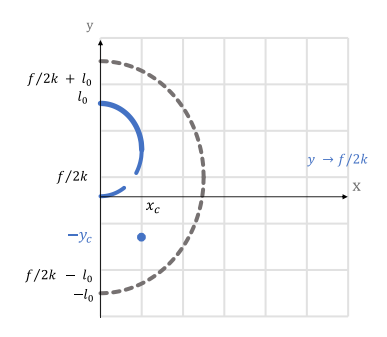


Fig. 7: Imperfect Pitchfork bifurcations

#### 3. Experiment

Two identical springs are used in our setup, attached to a polished surface using corks and screws. The setup can be used horizontally or vertically with attached weights for different conditions (Fig.8). The most important factors are studied in figures (9-11).



Fig. 8: Experimental setup

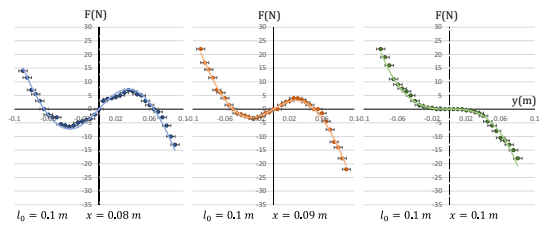


Fig. 9: F-y graph for different x values

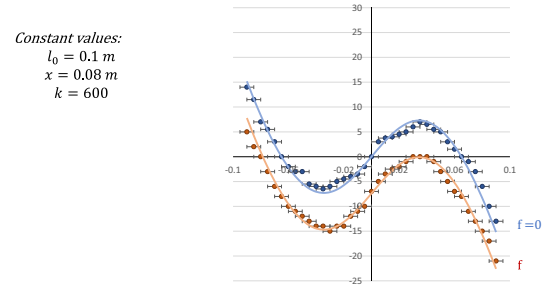


Fig.10: F-y graph for different f values

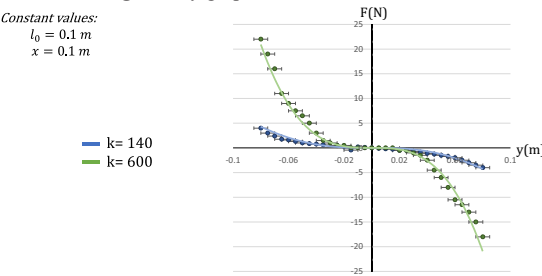


Fig. 11: F-y graph for different k values

#### 4. Conclusion

To study this problem Hooke's law and simple trigonometry were used to create an equation for net force. Then the hysteresis behavior in the system was analyzed. Further developed the equation to investigate bifurcations in the system and the spring bending force was calculated. The spring constant of different springs were measured experimentally .To minimize friction losses a polished surface was used then we used screws to allow for a full range of motion. Different weights were attached to the springs for achieving constant force.

- [1] J. J. Bissell and A. M. Nagaitis. Perfect and imperfect pitchfork bifurcations in a V-shaped spring-mass system: Comment on "Hysteresis in a simple V-shaped spring-mass system" [Am. J. Phys. 89, 663–665 (2021)]. Am. J. Phys. 91, 8, 659-660 (2023).
- [2] J. J. Bissell. Bifurcation, stability, and critical slowing down in a simple mass–spring system. Mech. Res. Commun. 125, 103967 (2022)
- [3] C. Ong. Hysteresis in a simple V-shaped spring-mass system. Am. J. Phys. 89, 7, 663-665 (2021)
- [4] Keller, S., & Gordon, A. (2010). Stress approximation technique for helical compression springs subjected to lateral loading

## STATIC SPEAKER

Javad Khoramdel , University of Khajeh Nasir co-authors: Foojan Norouzi kia , Ali Soleimani , Majid Zare, Hamed Shadkam

#### ABSTRACT

ARTICLE INFO

 $Participated in IPT/IRPT\,2018$ 

Supervisor Dr. A. Izadi

Accepted by Ariaian Young Innovative

Minds Institute, AYIMI

http://www.ayimi.org,info@ayimi.org

ound is a vibration that propagates as wave of pressure and needs a medium to be transmitted. At first, let's have a look at speakers and see how they work. What we are going to do, is using heat to produce and amplify sound. This approach leads to a phenomenon called "thermoacoustics effect". This effect can be observed in glass blowers, where blowing a hot bulb at the end of a cold narrow bulb produces sound. To investigate the parameters in this phenomenon, our data have been collected and analyzed from several experiments.

Keywords: Sound Waves, Vibration, Thermoacoustic Effect, amplify Sound

#### 1. Introduction

Sound is a vibration that propagates as wave of pressure and needs a medium to be transmitted. At first, let's have a look at speakers and see how they work.

As shown in figure (1), it consists of a circular magnet which is the North Pole. Within the cone, there is another magnet which is the South Pole, surrounded by the voice coil. Suspension (spider) supports whatever that is underneath it and allows the cone to move freely up and down.



#### How does it exactly work?

As we know, there is a magnetic field between the magnets, so if we put in current in the coil, based on the right-hand rule, we will have a force in a direction (upwards or downwards). Now if we change the direction of our current the force will be in the opposite direction of what it used to be. If we continue changing the direction of the current, the voice coil will keep moving up and down as well as the cone. For having this movement, we have to connect the coil to the AC supply so that it can have a particular frequency.

#### But how can we hear the sound?

As mentioned before, the cone is attached to the coil, so they have an equal vibration. This movement of the cone, pushes the air and makes what it's called "compression waves", and this is actually the sound waves that we can hear

What we are going to do, is using heat to produce and amplify sound. This approach leads to a phenomenon called "thermoacoustics effect". This effect can be observed in glass blowers, where blowing a hot bulb at the end of a cold narrow bulb produces sound.

#### 2. Theory

Sound is a wave of pressure, which means periodic change in pressure is needed to produce sound. Since common speakers are used in air and the medium is gas in this case, we focus on propagation of sound wave in air without loss of generality. From thermodynamics we know that pressure of a gas is proportional to its temperature for an ideal gas, and depends on temperature in more general case for real gases according to Van Der Waals equation. This is the point, we instead of changing pressure frequently to produce sound, we can change temperature of air near our device and change in temperature will result in change in pressure, so we can produce sound by changing temperature frequently. Increasing temperature of air requires thermal energy to increase internal energy of medium. According to thermodynamics' first law:

$$\delta U = \delta O - \delta W \tag{1}$$

$$\delta U = V \delta p + p \delta V \tag{2}$$

Where "U" is internal energy of system, "Q" represents heat transferred to the system and "W" is worked done on system.

Thermoacoustics speaker has no moving parts, so if we assume control volume is volume in semi\_sphere of radius "r" on top of our speaker, there shouldn't be any mechanical work on boundary, so there will be no works an also no change in volume.

$$\delta U = \delta Q \tag{3}$$

$$\delta U = V \delta p \ (Eq. 4) \tag{4}$$

We found out that we need a heat source which can frequently heat up the system and cool it down. We are going to use electrical power and Joule heating effect as heat source. When the current I is passed through a resistor, it makes the resistor hot and the heat coming off the resistor flows out into the air. The energy used by the resistor is converted entirely to heat. As we told before, we don't need to just increase temperature and also need to cool it down and do it frequently. If we use DC current, it just heats up the device and then air, so we can't produce sound in this way. But what if we apply AC current? An alternative current passes through the resistor and power produced is:

passes through the resistor and power produced is:  

$$P = \frac{1}{2}(RI^2 + RI^2\cos(2\omega t)) = P_{DC} + P_{AC}$$
(5)

Where, " $\omega$ " is frequency of AC current, "P" is power, "I" is maximum current, and "R" is resistance. As you can see, Power consists of two terms, the first term is called "DC power" and the second one is called "AC Power". DC power just heats up the device and as we mentioned before, this power can't produce sound, but AC power can do it. AC power changes with time and doesn't have constant heat production, which means it depends on time. So during a cycle. Air can be cooled through convection so temperature of air decreases when our device AC power is at its minimum value and increases, when AC power is maximum and near it. So what produces sound is AC power and DC power just increases temperature of our device. We need a resistor which has a high thermal effusivity (a measure which says how fast a material can transfer heat) and also be a perfect electric conductor. This resistor should be as thin as possible, if it's not, heat will be transferred by thermal conductivity between layers of resistors and it reduces speed of heat transfer. Heat is also transferred between layers of resistors through its thickness while our goal is to transfer heat to air, in other words resistor is used as a heat sink which needs. Resistor should transfer heat to air and it occurs through convection so it must have a surface to be able to transfer heat through convection better. We offer to use graphene as resistor. But why graphene? Graphene is an allotrope of carbon and consists of layers, in each layer carbon atoms are bonded to each other with covalent bonds and layers are connected to each other due to van der Waals force. So we expect thermal conductivity not to be isotropic and changes with direction. In fact thermal conductivity K reaches about 3000 W m<sup>1</sup> K<sup>-1</sup> in the parallel to planes direction, and 5 W m<sup>-1</sup> <sup>1</sup> K<sup>-1</sup> orthogonally. So when number of layers decreases, we can assume that heat transfer in graphene occurs only in parallel to plane and we can neglect it. So if we use thin graphene layer, we can assume that as electric current passes through graphene, it heats up graphene and all heat is in a thin layer of graphene and this heat is transferred to air through convection and heat transferred from the surface which is in contact with air is to other layers is negligible, so efficiency increases. Graphene also has a high thermal effusivity which means it can transfer heat faster in comparison with lots of materials.

Heat transferred to the system is summation of heat transferred to graphene and air:

$$\delta Q = \delta Q_a + \delta Q_g \tag{6}$$

also we know that:

$$\delta Q_a = \frac{C_a}{C_a + C_g} \delta Q \tag{7}$$

$$\delta Q_g = \frac{C_g}{C_a + C_g} \delta Q \tag{8}$$

$$C_g = m_g c_{p,g} = \rho_g S d_g c_{p,g} \tag{9}$$

$$C_a = m_a c_{p,a} = \rho_a S d_a c_{p,a} \tag{10}$$

Where C is thermal conductivity in constant pressure, S is surface, d is thickness, c is specific heat capacity and  $\rho$  is density and index "a" is for air and g is for graphene. Since surface of air which is in contact with graphene is equals to graphene surface, so we didn't use index for S."  $d_a^{\alpha}$  is skin depth of the thermal boundary layer of air and defined as a distance where if temperature of heat source changes, after  $\frac{1}{f}$  seconds, air is affected by change in temperature and f is frequency.

$$d_a = \sqrt{\frac{k_a}{\rho_a c_{p,a}}} \tag{11}$$

If we use this in Eq.7 we will have:

$$C_a = e_a. S. \omega^{-\frac{1}{2}} \tag{12}$$

Where "e" is thermal effusivity. We can define effusivity for graphene as:

$$e_g = \rho_g d_g c_{p,g} \sqrt{\omega} \tag{13}$$

Which has same dimension with  $e_{a}$ 

So we have:

$$\delta Q_a = \frac{e_a}{e_a + e_g} \delta Q = \frac{e_a}{e_a + e_g} \cdot \frac{P_{AC}}{f}$$
 (14)

Using Eq.3, Eq.4 and Eq.14 at the same time will give us:

$$\delta p = \frac{e_a}{e_a + e_g} \cdot \frac{P_{AC}}{f} \cdot \frac{1}{V} \tag{15}$$

"V" is volume of control volume which we defined before as a hemisphere, so:

$$V = \frac{2}{3}\pi r^3 \tag{16}$$

Since wave is sonic, it travels at speed of sound. We want to assume our speaker to be a point source. This requires dimensions of graphene be much smaller than wavelength. So if we want to produce a sound of frequency 100 Hz, speed of sound in room temperature and 1 atmosphere pressure is approximately 300 m/s, so wavelength will be 3 meters and that will be surely much greater than dimensions of graphene we will use. So this can be a reasonable assumption to think of our speaker as a point source. If we assume speed of sound as "Va", then after 1/f seconds, wave will reach the distance "r":

$$r = \frac{Va}{f} \tag{17}$$

$$r = \frac{Va}{f}$$

$$V = \frac{2}{3}\pi \left(\frac{Va}{f}\right)^{3}$$

$$(18)$$

$$\delta p = \frac{e_a}{e_a + e_a} \cdot \frac{3P_{AC}f^2}{2\pi V a^3} \tag{19}$$

Eq. 19 gives us a relation between change in pressure and input power. But it needs correction. As sound wave travels through a medium, its energy attenuates due to viscosity and amplitudes of wave decreases exponentially with distance from point source due to formula:

$$A = A_0 e^{-\alpha z} \tag{20}$$

A" is reduced amplitude,  $A_0$  is unattenuated amplitude of the propagating wave at some location, "z" is the distance which sound traveled and  $\alpha$  is attenuation coefficient which probably depends on Prandtl number and viscosity of medium. The Eq.19 says that pressure is proportional to AC power and since AC power is a cosine wave, there will be an extreme point for AC power (and also pressure)

$$t = T = \frac{1}{2f}$$
 (here frequency of AC power is 2f)

After this time, wave reaches  $r_0$  and has a maximum

$$r_0 = \frac{Va}{2f} \tag{21}$$

So  $A_0$  must have its maximum value  $(A_0 = 1)$  at this distance and must decrease as wave propagates in air. So we can assume that: $A_0 = r_0 \cdot F(r)$  and  $r_0 F(r_0) = 1$ . So we can correct Eq.20:

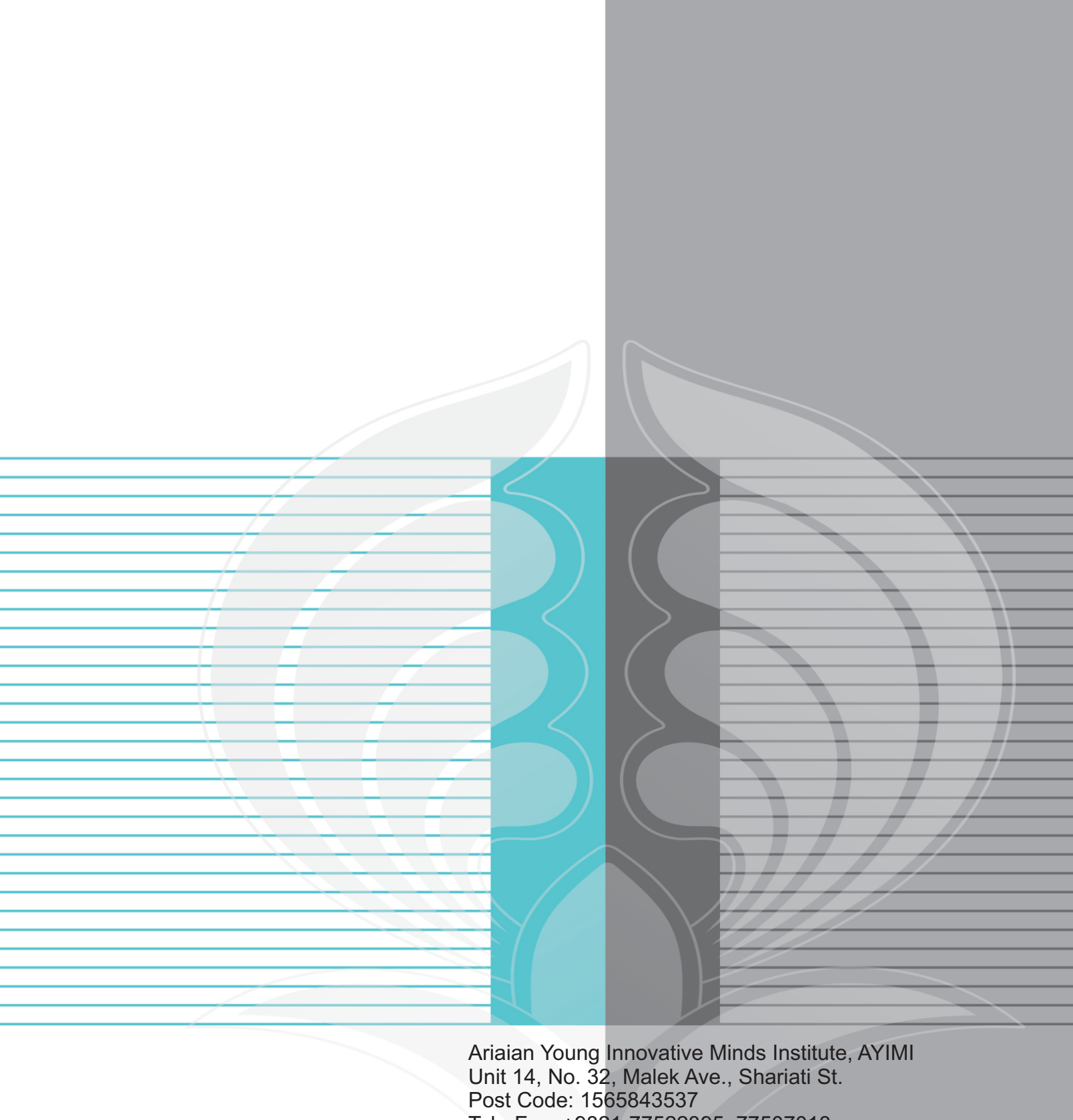
$$\delta p = \frac{e_a}{e_a + e_g} \cdot \frac{3P_{AC}f^2}{2\pi V a^3} A_0 e^{-\alpha z} = \frac{e_a}{e_a + e_g} \cdot \frac{3P_{AC}f}{4\pi V a^2} r_0 F(r) e^{-\alpha z}$$
(22)

We used AC current of frequency  $\omega$  and AC power is  $2\omega$ . Since pressure is proportional to AC power, sound wave will have frequency 2 times of input frequency. Since oscillator can produce AC current of frequency 0 to even more than 20 KHz, this device can produce sound of any frequency. This Thermoacoustic device doesn't have any moving parts and can produce sound of all frequency and is limited just by frequency of oscillator. In Eq.19 we didn't consider dissipation of energy. Here we have heat transfer and air moves as its temperature and density changes, so energy dissipation may depends on Prandtl number. Since sound propagates through a fluid, it may also depends on viscosity of fluid. But Eq.22 includes energy attenuation and as we mentioned before,  $\alpha$  probably depends on Prandtl and viscosity of medium.

#### Future Work:

- 1- Using analogy between Stokes' second problem to derive energy dissipation and skin depth thermal boundary layer.
- 2- Simulating device in Comsol to discuss about heat transfer in graphene and air.
- 3- Doing experiments on experimented results.
- 4- Amplifying sound

- [1] Michael A. Boles and Yungus A. Cengel, Thermodynamics: An Engineering Approach
- [2] L. E. Kinsler, A. R. Frey, A. B. Coppens, and J. V. Sanders, Fundamentals of Acoustics
- [3] J. H. Lienhard IV and J. H. Leinhard V, A Heat Transfer Textbook
- [4] Lord Rayleigh, The theory of sound, 2ndedition, Dover, New York
- [5] Electric power systems: a conceptual introduction by Alexandra von Meier
- [6] Frank P. Incropera, Introduction to heat transfer
- [7] 5.H. Su Kim, H. Sung Bae, J. Yu, and S. Y. Kim, Sci. Rep. 6, 26825 (2016). https://doi.org/10.1038/srep26825,
- [8] 6.X. Shen, Z. Wang, Y. Wu, X. Liu, Y.-B. He, and J.-K. Kim, Nano Lett. 16(6), 3585 (2016). https://doi.org/10.1021/acs.nanolett.6b00722,
- [10] M. S. Heath & D. W. Horsell, Multi-frequency sound production and mixing in graphene 11http://www.personal.psu.edu/hmj5052/Assignment.html



Tel - Fax: +9821-77522395, 77507013

Tehran/Iran

URL: http://www.ayimi.org

http://journal.ayimi.org

Email: info@ayimi.org